Open Journal of Mathematical Sciences

PSR Press

Article

Fractional predator-prey system under allee effect and anti-predator feedback

Sarita Pippal[1,*] and Jasmine Sati[2]

[1] Department of Mathematics, Panjab University, Chandigarh, India
[2] Center for Nuclear Medicine, Panjab University, Chandigarh, India
* Correspondence: saritamath@pu.ac.in

Received: 15 Nov 2025; Revised: 13 Dec 2025; Accepted: 04 Mar 2026; Published: 14 Aug 2026

Abstract: A *fractional-order predator–prey model* (FOPPM) based on the Caputo derivative of order α ($0 < \alpha \leq 1$) is developed to examine the joint influence of a *strong Allee effect* in the prey and a *nonlinear anti-predator feedback* acting on the predator. The formulation couples cubic prey growth and bilinear predation with a saturating feedback loss, thereby representing threshold-dependent recovery, trophic conversion, and density-dependent behavioural regulation. The system admits three boundary equilibria, while coexistence equilibria are determined by a corrected cubic algebraic equation. Its discriminant classifies one- and three-real-root regimes, but ecological feasibility further requires $A < X^* < K$, $Y^* > 0$, and $kmX^* - d > 0$. Nullcline geometry shows that at most two roots can be biologically feasible; the actual number is therefore established by direct root filtering for each parameter set. Local stability is characterised through the Jacobian $\mathcal{J}(E^*)$ and the classical eigenvalue test for integer-order dynamics, while the fractional-order model requires satisfaction of Matignon's criterion $|\arg(\lambda_i)| > \frac{\alpha\pi}{2}$, $i = 1, 2$. The coexistence equilibrium may switch between stability and instability under variations in carrying capacity K, Allee threshold A, interaction rate m, or feedback intensity ε. Because the Jacobian eigenvalues do not depend on α, fractional memory does not rotate them; instead, decreasing α widens the admissible Matignon sector and changes the rate and shape of transient relaxation. A weighted population estimate establishes positivity, uniform boundedness, and global existence. Since the extinction equilibrium is always locally stable under a strong Allee effect, coexistence cannot be globally attractive on the entire positive quadrant. A Volterra-type logarithmic functional is therefore formulated as a basin-restricted Mittag–Leffler certificate on positively invariant sets separated from the coordinate axes. The theoretical results are tested with a fractional Adams–Bashforth–Moulton predictor–corrector (ABM–PC) scheme. A grid-refinement study gives observed orders 1.91, 1.90, and 1.96 for $\alpha = 0.9$, consistent with the expected order $\min\{2, 1 + \alpha\}$. An independent $\alpha = 1$ comparison with a high-accuracy Runge–Kutta solution gives maximum componentwise errors below 3.5×10^{-4}. Parameter sweeps across $(K, A, m, \varepsilon, \alpha)$ then quantify changes in feasibility, stability, and transient persistence. For $\alpha = 1$, a trace-zero crossing with positive determinant and transversality is the classical Hopf candidate. For $0 < \alpha < 1$, crossing the Matignon boundary is instead a fractional stability-sector transition; it is not, by itself, a Hopf bifurcation. Moreover, autonomous Caputo systems of non-integer order do not possess exact nonconstant periodic solutions, so the computed oscillations are interpreted as memory-dependent transients rather than limit cycles. Overall, the FOPPM provides a coherent framework for studying memory, Allee thresholds, and behavioural feedback within one model. Corrected equilibrium algebra, explicit feasibility filtering, fractional stability theory, reproducible convergence checks, and regenerated simulations together distinguish true asymptotic conclusions from finite-time memory effects.

Keywords: fractional-order system, allee effect, anti-predator feedback, predator-prey dynamics

MSC: 34A34, 65L05, 92D30.

1. Introduction

The study of organism abundance, distribution, and their influence on the environment through mathematical modeling has gained considerable attention. One of the earliest and most influential

formulations is the classical Lotka–Volterra predator–prey (LVPP) model [1,2], which introduced the concept of oscillatory population dynamics arising from species interactions. Although the LVPP model effectively captures predator–prey (PP) cycles, it neglects density-dependent regulation and several ecological complexities. These limitations were addressed in subsequent studies [3,4], which incorporated logistic growth and carrying-capacity effects to enhance ecological realism.

To improve biological realism, various extensions of the LVPP model have been proposed, incorporating mechanisms such as predator functional responses, prey refuge, time delays, stage structure, and memory (fractional) effects. Prominent examples include Holling-type (HT) functional responses [5,6] and ratio-dependent (RD) models [7]. Kar [8] analyzed an HT-II predator–prey model incorporating prey refuge and examined its local and global stability properties.

Several studies have explored the influence of prey refuge (PR) on population dynamics. The term refers to a fraction of the prey population that is temporarily or permanently protected from predation due to environmental heterogeneity, spatial hiding, behavioral defenses, or structural shelters such as burrows or vegetation. In mathematical models, this concept is typically represented by a refuge parameter (ρ), denoting the proportion of prey inaccessible to predators in PP systems. Tripathi et al. [9] analyzed a density-dependent delayed PP system with a Beddington–DeAngelis (BDA) functional response and demonstrated that PR can stabilize population oscillations. Wei and Fu [10] investigated the occurrence of Hopf bifurcation (HOB) in a similar model with prey stage structure and showed that the refuge parameter plays a crucial role in delaying or preventing population cycles. Huang et al. [11] examined an HT-III response incorporating PR and found that the refuge provides a stabilizing mechanism against predator overexploitation.

Furthermore, Ma and collaborators [12,13] extended the analysis to LV-type systems that include mutual interference among predators, concluding that greater refuge availability enhances system stability and biodiversity persistence. Tang et al. [14] performed a global stability analysis for an HT-II model with constant PR, confirming the refuge's stabilizing effect. Bianca and co-authors [15,16] developed a thermostatted kinetic-theory framework to describe complex biological systems with particle refuges, including applications to tumour dynamics.

A phenomenon in population ecology in which the individual fitness or per-capita growth rate increases with population density when the density is low is known as the *Allee effect (AE)*, first identified by W. C. Allee [17]. In other words, populations may struggle to grow or even decline when their numbers fall below a critical threshold. This effect can arise from various biological mechanisms, such as difficulties in finding mates, cooperative defense, social facilitation, or genetic inbreeding at low densities [18]. Terry extended the classical predator-prey framework by incorporating an AE component in the predator's reproduction term, demonstrating that the AE can stabilize or destabilize coexistence equilibria depending on parameter values.

Mathematically, the AE modifies the classical logistic growth law by introducing a critical population threshold A (the *Allee threshold*), below which the population growth rate becomes negative. The generalized Allee-type growth model is given by

$$\frac{d\mathcal{N}}{dt} = \mathcal{R}\mathcal{N}\left(1 - \frac{\mathcal{N}}{K}\right)\left(\frac{\mathcal{N}}{A} - 1\right), \tag{1}$$

where $\mathcal{N}$ denotes the population size, $\mathcal{R}$ is the intrinsic growth rate, and K is the carrying capacity. This strong-Allee parametrisation is defined only for $A > 0$ and does not possess a finite limit as $A \to 0^+$. For comparison, the corresponding model without an Allee factor is the classical logistic equation:

$$\frac{d\mathcal{N}}{dt} = \mathcal{R}\mathcal{N}\left(1 - \frac{\mathcal{N}}{K}\right). \tag{2}$$

For $A > 0$, this equation specifically represents a *strong AE*: the per-capita growth rate is negative for $0 < \mathcal{N} < A$. A weak AE requires a different growth factor whose per-capita rate remains positive near zero. As shown in Figure 1, the AE alters the logistic curve by introducing a depensation region near zero population

density. When the initial population satisfies $N(0) < A$, extinction occurs, whereas $N(0) > A$ leads to growth toward the carrying capacity K. The model admits three equilibria:

$$\mathcal{N}_1 = 0 \text{ (extinction)}, \qquad \mathcal{N}_2 = A \text{ (unstable threshold)}, \qquad \mathcal{N}_3 = K \text{ (stable equilibrium)}. \tag{3}$$

Populations below the Allee threshold ($\mathcal{N} < A$) decline to extinction, while those above it ($\mathcal{N} > A$) approach K.

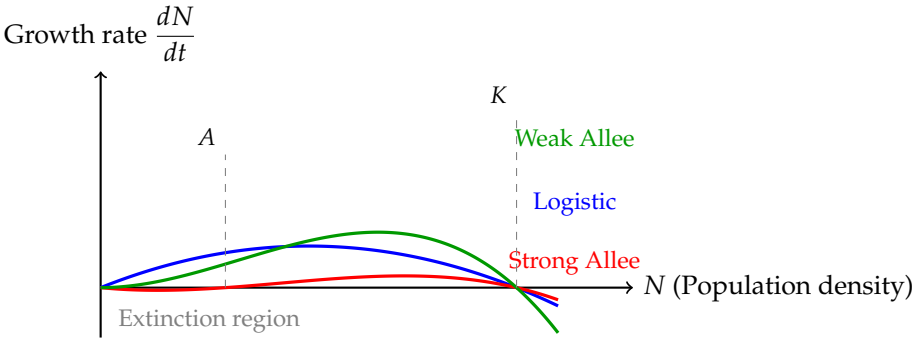

Figure 1. Population growth rate versus population density for logistic and Allee-type dynamics. The parameter A denotes the critical Allee threshold and K represents the carrying capacity. Below A, population growth is negative, indicating an extinction region

Incorporating Allee mechanisms into population models introduces threshold phenomena: below a critical density, an otherwise viable population may decline to extinction, while above the threshold it tends toward the carrying capacity. Many studies have examined how AEs interact with predation, refuge, and other nonlinearities to produce bistability, saddle-node or transcritical bifurcations, and more complex dynamical regimes. The presence of an Allee threshold is particularly relevant in conservation biology and invasion ecology because it determines extinction risk and invasion success.

Recent years have seen a surge of interest in fractional-order models (FOMs), which introduce memory and hereditary effects via fractional derivatives (FDs). Fractional formulations are natural when past states influence current rates, for example due to physiological memory or cumulative environmental effects. Several studies have extended PP and other ecological models to fractional orders, exploring stability, bifurcation, and control in the presence of memory terms [19–21]. In the context of the Benjamin–Bona–Mahony (BBM) and Benjamin–Bona–Mahony–Burgers (BBMB) types of partial differential equations (PDEs), fractional time or space derivatives capture anomalous dispersion and nonlocal dynamics in wave propagation [22,23]. More recent fractional PP analyses include models that combine delay differential equations (DDEs), cannibalism, or PR with fractional dynamics [24–27].

Among these, FOMs have been developed to better capture the memory and hereditary properties inherent in biological systems with Allee-type feedback. For instance, Rayungsari et al. [24] analyzed a fractional-order predator–prey model (FOPPM) incorporating cannibalism and PR, while Zhang and Muhammadhaji [25] considered a delayed fractional-order model with stage-structured prey and cannibalism. Furthermore, Gao et al. [26] and Wang and Meng [28] explored fractional predator–prey systems exhibiting bifurcation and complex dynamics under the combined influence of refuge, fear effects, and economic thresholds. In addition, Lu et al. [29] and Liu et al. [27] investigated chaos and incommensurate fractional dynamics in ecological systems, revealing that fractional memory and Allee-type feedback significantly enrich the system's dynamical behavior.

Sun et al. [30] developed a prey-guided anti-predator PP model to capture behavioral feedback between prey abundance and predator activity. In their formulation, the anti-predator response was modeled as a dynamic function driven by prey density, reflecting the tendency of predators to adjust their hunting intensity according to prey availability. Their analytical and numerical results revealed multiple dynamical regimes, including stable coexistence, limit cycles, and complex oscillations. The inclusion of prey-guided anti-predator behavior significantly altered classical predator–prey dynamics by delaying predator responses and modifying invasion thresholds. These findings emphasized the ecological importance of behaviorally mediated feedback

in maintaining population balance and preventing extinction, providing a biologically realistic foundation for subsequent model extensions involving additional nonlinear mechanisms such as AEs and fractional memory dynamics.

The present model is motivated by the prey-guided anti-predator framework of Sun et al. [30], who showed that behavioural feedback between prey abundance and predator response can substantially modify classical PP dynamics. Building on that formulation, we combine two additional mechanisms within a common analytical setting. First, the prey population experiences a strong AE, represented by the cubic growth term $r\,\mathcal{X}\left(1-\frac{\mathcal{X}}{K}\right)\left(\frac{\mathcal{X}}{A}-1\right)$, which introduces a critical density threshold below which the prey cannot recover and extinction occurs [17,18]. This captures depensation and small-population vulnerability. Second, to account for the nonlocal temporal dependence inherent in biological interactions, we extend the system to fractional-order dynamics in the Caputo sense ($0 < \alpha \leq 1$) [22,23,31,32]. The fractional derivative characterizes memory effects, implying that current growth and interaction rates depend on the entire history of the populations rather than instantaneous values alone. The nonlinear interaction functions $\Phi(\mathcal{X}) = m\mathcal{X}$, and $F(\mathcal{Y}) = \frac{b\mathcal{Y}}{1+c\mathcal{Y}}$, represent a linear predation response and a saturating anti-predator feedback, respectively, following the behavioral mechanism proposed by Sun et al. [30]. This formulation enables a controlled analysis of how the AE, feedback saturation, and fractional memory modify feasibility, invasion thresholds, local stability, and transient oscillations.

1.1. Novelty and key contributions of this work

Strong Allee thresholds, anti–predator behavioural feedback, and fractional–order memory have each been investigated independently in ecological modelling; see, for example, Allee-induced collapse in prey populations [18,33], behaviourally mediated predator suppression [34,35], and fractional–order predator–prey dynamics [32]. Their *joint interplay* is less developed than each mechanism separately. The resulting combination raises distinct questions about whether algebraic roots are ecologically feasible, how the fractional stability sector differs from the classical criterion, and how memory alters finite-time persistence without changing equilibrium locations.

The present work introduces a unified fractional predator–prey model in which *all three regulatory mechanisms act simultaneously*. This coupling produces threshold and feedback effects not represented simultaneously in classical Lotka–Volterra extensions [36,37], fractional models without Allee effect [32], or integer–order Allee-feedback systems [38].

The main novelties of our study are summarized below:

1. *Unified model formulation:* We formulate a Caputo fractional predator–prey system combining (i) strong Allee effect in prey, (ii) prey-guided nonlinear anti-predator feedback, and (iii) memory-dependent interaction terms. Their roles remain separately identifiable in the equilibrium and stability calculations.
2. *New analytical results:* We derive the corrected cubic equilibrium equation, its discriminant and feasibility conditions, and combine them with boundary and coexistence stability criteria. The nullcline geometry additionally limits the number of biologically feasible coexistence states.
3. *Memory-mediated dynamics:* The fractional order α regulates relaxation rate and transient amplitude without moving equilibria or Jacobian eigenvalues. We distinguish classical Hopf candidates, fractional stability-sector crossings, and long transient coexistence near the extinction threshold [39,40].
4. *Biological insight and applicability:* Our results show that fractional memory can *delay an observed finite-time decline* under strong Allee pressure, but it does not remove the stable extinction basin. This distinction is important when interpreting short observation windows in species recovery studies where behaviour and memory may play a significant role [18,35].

In summary, unlike previous studies that examined these mechanisms separately, our model resolves *coupled feasibility and stability transitions* arising from the *coupling of Allee effect, nonlinear anti-predator feedback, and fractional memory*. This provides a mathematically auditable framework for assessing population persistence under multiple nonlinear ecological pressures.

2. Preliminaries

Only concepts essential for the analysis of the proposed fractional predator–prey model are recalled. Detailed theory may be found in the books by Podlubny [23] and Kilbas et al. [22].

Definition 1 (Caputo fractional derivative)**.** For $0 < \alpha < 1$ and $f \in C^1$,

$$ {}^{C}D_t^{\alpha} f(t) = \frac{1}{\Gamma(1-\alpha)} \int_0^t \frac{f'(\tau)}{(t-\tau)^{\alpha}} d\tau, \tag{4} $$

which admits integer-order initial conditions. The Riemann–Liouville form is

$$ {}^{RL}D_t^{\alpha} f(t) = \frac{1}{\Gamma(1-\alpha)} \frac{d}{dt} \int_0^t \frac{f(\tau)}{(t-\tau)^{\alpha}} d\tau, \tag{5} $$

and the two operators satisfy

$$ {}^{C}D_t^{\alpha} f(t) = {}^{RL}D_t^{\alpha}[f(t) - f(0)]. \tag{6} $$

Definition 2 (Fractional dynamical system)**.** A system of order $0 < \alpha \leq 1$ in $\mathbb{R}^n$ is written as

$$ {}^{C}D_t^{\alpha} \boldsymbol{U}(t) = \boldsymbol{F}(\boldsymbol{U}(t)), \qquad \boldsymbol{U} = (u_1, \ldots, u_n)^T \in \mathbb{R}^n. \tag{7} $$

For $\alpha = 1$,

$$ \dot{\boldsymbol{U}} = \boldsymbol{F}(\boldsymbol{U}). \tag{8} $$

Definition 3 (Jacobian)**.** For $\boldsymbol{F} = (f_1, \ldots, f_n)^T \in C^1$,

$$ \boldsymbol{J}(\boldsymbol{U}) = \left[\frac{\partial f_i}{\partial u_j} \right]_{i,j=1}^{n}, \tag{9} $$

which linearizes system (7) at equilibrium $\boldsymbol{U}^*$. For $n = 2$, $\boldsymbol{U} = (\mathcal{X}, \mathcal{Y})$,

$$ \boldsymbol{J}(\boldsymbol{U}) = \begin{pmatrix} f_{1\mathcal{X}} & f_{1\mathcal{Y}} \\ f_{2\mathcal{X}} & f_{2\mathcal{Y}} \end{pmatrix}. \tag{10} $$

Theorem 1 (Matignon fractional stability)**.** *Consider the linearization*

$$ {}^{C}D_t^{\alpha} \boldsymbol{u} = \boldsymbol{J}\boldsymbol{u}, \qquad 0 < \alpha \leq 1, \tag{11} $$

with eigenvalues $\lambda_i \in \sigma(\boldsymbol{J})$. Then

$$ |\arg(\lambda_i)| > \frac{\alpha\pi}{2} \iff \boldsymbol{U}^* \text{ is locally asymptotically stable.} \tag{12} $$

For $\alpha = 1$,

$$ \Re(\lambda_i) < 0. \tag{13} $$

Definition 4 (Predator–prey system)**.** Let prey $\mathcal{X}(t)$ and predator $\mathcal{Y}(t)$ dynamics be

$$ \dot{\boldsymbol{U}} = \begin{pmatrix} f(\mathcal{X}) - g(\mathcal{X}, \mathcal{Y}) \\ \eta g(\mathcal{X}, \mathcal{Y}) - d\mathcal{Y} \end{pmatrix}, \qquad \boldsymbol{U} = (\mathcal{X}, \mathcal{Y})^T. \tag{14} $$

The classical Lotka–Volterra model satisfies

$$ f(\mathcal{X}) = r\mathcal{X}, \qquad g(\mathcal{X}, \mathcal{Y}) = a\mathcal{X}\mathcal{Y}. \tag{15} $$

Lemma 1 (Real root structure of a cubic polynomial [41])**.** *Consider the cubic polynomial*

$$ P(x) = a_3x^3 + a_2x^2 + a_1x + a_0, \qquad a_3 \neq 0, \tag{16} $$

with discriminant

$$ \Delta = 18a_3a_2a_1a_0 - 4a_2^3a_0 + a_2^2a_1^2 - 4a_3a_1^3 - 27a_3^2a_0^2. \tag{17} $$

The sign of Δ determines the real-root structure of $P(x)$:

1. *If $\Delta > 0$, the cubic polynomial has three distinct real roots.*
2. *If $\Delta = 0$, the polynomial possesses multiple real roots (double or triple root).*
3. *If $\Delta < 0$, the polynomial has exactly one real root and one complex conjugate pair.*

3. Model formulation and numerical simulation

Let $\mathcal{X}(t)$ and $\mathcal{Y}(t)$ denote prey and predator densities at time $t > 0$. The interaction between species is governed by a Caputo fractional–order system of order $0 < \alpha \leq 1$:

$$^{C}D_t^{\alpha}\mathcal{X}(t) = r\mathcal{X}(t)\left(1 - \frac{\mathcal{X}(t)}{K}\right)\left(\frac{\mathcal{X}(t)}{A} - 1\right) - \Phi(\mathcal{X}(t))\,\mathcal{Y}(t), \tag{18}$$

$$^{C}D_t^{\alpha}\mathcal{Y}(t) = k\,\Phi(\mathcal{X}(t))\,\mathcal{Y}(t) - d\,\mathcal{Y}(t) - \varepsilon\,F(\mathcal{Y}(t))\,\mathcal{X}(t). \tag{19}$$

Nonlinear interaction functions:

$$\Phi(\mathcal{X}) = m\mathcal{X}, \qquad F(\mathcal{Y}) = \frac{b\mathcal{Y}}{1 + c\mathcal{Y}}, \qquad m, b, c > 0. \tag{20}$$

Substituting (20) into the system gives

$$^{C}D_t^{\alpha}\mathcal{X}(t) = r\mathcal{X}(t)\Big(1 - \frac{\mathcal{X}(t)}{K}\Big)\Big(\frac{\mathcal{X}(t)}{A} - 1\Big) - m\mathcal{X}(t)\mathcal{Y}(t), \tag{21}$$

$$^{C}D_t^{\alpha}\mathcal{Y}(t) = km\mathcal{X}(t)\mathcal{Y}(t) - d\mathcal{Y}(t) - \varepsilon\,\frac{b\mathcal{Y}(t)}{1 + c\mathcal{Y}(t)}\,\mathcal{X}(t). \tag{22}$$

Biological implications:

$$0 < A < K \Rightarrow \text{strong Allee threshold}, \qquad \mathcal{X}(t) < A \;\Rightarrow\; {}^{C}D_t^{\alpha}\mathcal{X}(t) < 0,$$

$$\alpha < 1 \Rightarrow \text{memory effect, slower recovery, nonlocal dependence.}$$

Ecological memory interpretation follows [22,23,31,32], and Allee–driven prey growth follows [17,18,26, 28].

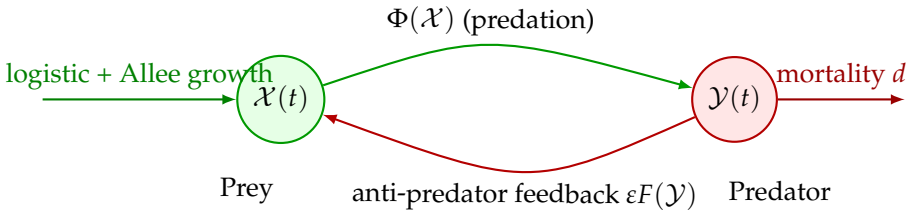

Figure 2. Schematic representation of the fractional predator–prey system with Allee effect and anti-predator feedback

3.1. Parameter assumptions

All parameters are assumed to be positive, i.e., $r, K, A, k, d, m, b, c > 0$ and $\varepsilon \geq 0$. The biological restriction $0 < A < K$ ensures that the Allee threshold lies below the carrying capacity so that prey recovery occurs only when $\mathcal{X} > A$. The control variable ε regulates the nonlinear anti–predator inhibition: $\varepsilon = 0$ removes behavioural suppression, whereas $\varepsilon > 0$ introduces density-dependent feedback; temporal memory is controlled independently by α. The dimensionless intervals used for the analytical sweeps and simulations are summarised in Table 1; they are illustrative ranges informed by standard predator–prey scales in [11,32].

Table 1. Model parameters and their ecological interpretation for the fractional predator–prey system with Allee effect

Symbol	*Description*	*Range*	*Reference*
r	Prey intrinsic growth rate	0.5–2.0	Freedman [36], Chattop. [43]
K	Carrying capacity	1–12	May [37], Murdoch [44]
A	Allee threshold	$0.1K$–$0.4K$	Courchamp [33], Chattop. [43]
m	Predation intake rate	0.1–2.0	Holling [5], Rosenb. [45]
b	Saturation in feedback	0.1–1.0	Holling [5]
k	Conversion efficiency	0.3–0.9	Holling [5]
d	Predator mortality rate	0.1–0.5	Freedman [36]
ε	Anti–predator feedback intensity	0–1	*This study*
α	Caputo derivative order	$0 < \alpha \leq 1$	Diethelm [46]

The vector field is quasipositive because $\mathcal{F}_1(0,\mathcal{Y}) = 0$ and $\mathcal{F}_2(\mathcal{X},0) = 0$. Consequently, the positive orthant $\mathbb{R}^2_{\geq 0}$ is invariant (cf. Definition 2). Specific numerical values are stated with each simulation, follow Table 1, and lie within the reported sweep intervals.

4. Dynamical analyses of system

4.1. Well-posedness and qualitative properties

Theorem 2 (Well-posedness)**.** *For Eqs. (21) to (22) with Caputo order $0 < \alpha \leq 1$, parameters $r, K, A, k, d, m, b, c > 0$, $\varepsilon \geq 0$ and initial data $\mathcal{X}(0) = \mathcal{X}_0 \geq 0$, $\mathcal{Y}(0) = \mathcal{Y}_0 \geq 0$, the following hold:*

(i) *Local existence and uniqueness: Consider the fractional-order predator–prey system written in vector form as*

$$ {}^{C}D_t^{\alpha}\boldsymbol{\mathcal{U}}(t) = \boldsymbol{\mathcal{F}}\big(\boldsymbol{\mathcal{U}}(t)\big), \qquad \boldsymbol{\mathcal{U}}(t) = (\mathcal{X}(t),\mathcal{Y}(t))^{\top}, \quad 0 < \alpha \leq 1. \tag{23}$$

The nonlinear vector field is defined by

$$\boldsymbol{\mathcal{F}}(\mathcal{X},\mathcal{Y}) = \begin{pmatrix} r\mathcal{X}\left(1-\dfrac{\mathcal{X}}{K}\right)\left(\dfrac{\mathcal{X}}{A}-1\right) - m\mathcal{X}\mathcal{Y} \\ km\mathcal{X}\mathcal{Y} - d\mathcal{Y} - \varepsilon\dfrac{b\mathcal{X}\mathcal{Y}}{1+c\mathcal{Y}} \end{pmatrix}, \tag{24}$$

which is locally Lipschitz on $\mathbb{R}^2_+$ since all component functions are smooth on this domain.

Therefore, by the standard existence and uniqueness theorem for Caputo fractional differential equations, there exists a unique solution

$$\boldsymbol{\mathcal{U}}(t) = (\mathcal{X}(t),\mathcal{Y}(t))^{\top}, \tag{25}$$

defined on some interval $t \in [0,T)$ for any initial condition

$$\boldsymbol{\mathcal{U}}(0) = \boldsymbol{\mathcal{U}}_0 \in \mathbb{R}^2_+. \tag{26}$$

(ii) *Positivity: $\Phi(0) = F(0) = 0$ implies $\mathcal{X}(t), \mathcal{Y}(t) \geq 0$ for all $t \geq 0$; thus $\mathbb{R}^2_{\geq 0}$ is forward-invariant.*

(iii) *Uniform boundedness: There exist finite constants $C_{\mathcal{X}}, C_{\mathcal{Y}} > 0$ such that $0 \leq \mathcal{X}(t) \leq C_{\mathcal{X}}$, $0 \leq \mathcal{Y}(t) \leq C_{\mathcal{Y}}$ for all $t \geq 0$.*

(iv) *Global existence: Bounded trajectories prevent finite-time blow-up; hence the solution extends globally, i.e. $\boldsymbol{\mathcal{U}}(t) \in \mathcal{C}([0,\infty))$.*

Proof. Eqs. (21)–(22) are equivalent to the Volterra formulation

$$U(t) = U_0 + \frac{1}{\Gamma(\alpha)}\int_0^t (t-s)^{\alpha-1}\mathcal{F}(U(s))\,ds, \qquad U = (X,Y)^{\top}. \tag{27}$$

(i) *Local existence and uniqueness.* On any compact box $\mathcal{D}$ containing U_0, the vector field

$$\mathcal{F}(U) = \begin{pmatrix} \mathcal{F}_1(X,Y) \\ \mathcal{F}_2(X,Y) \end{pmatrix} = \begin{pmatrix} rX\left(1-\frac{X}{K}\right)\left(\frac{X}{A}-1\right) - mXY \\ kmXY - dY - \varepsilon\frac{bY}{1+cY}X \end{pmatrix}, \tag{28}$$

is C^1 and therefore locally Lipschitz:

$$\|\mathcal{F}(u_1) - \mathcal{F}(u_2)\| \leq L_{\mathcal{D}}\|u_1 - u_2\|, \qquad L_{\mathcal{D}} = \max\{B_{11}, B_{12}, B_{21}, B_{22}\}. \tag{29}$$

Define the associated integral operator

$$(\mathcal{T}U)(t) = U_0 + \frac{1}{\Gamma(\alpha)}\int_0^t (t-s)^{\alpha-1}\mathcal{F}(U(s))\,ds. \tag{30}$$

Using the standard fractional convolution bound,

$$\|\mathcal{T}U - \mathcal{T}V\|_\infty \leq \frac{L_{\mathcal{D}}T^\alpha}{\Gamma(\alpha+1)}\|U-V\|_\infty, \tag{31}$$

and selecting

$$T < \left(\frac{\Gamma(\alpha+1)}{L_{\mathcal{D}}}\right)^{1/\alpha},$$

makes $\mathcal{T}$ a contraction and guarantees a unique local solution.

(ii) *Positivity.* From (28),

$$\mathcal{F}_1(0,Y) = 0, \qquad \mathcal{F}_2(X,0) = 0 \qquad (X,Y \geq 0). \tag{32}$$

Thus, the system is quasi–positive.

The equivalent Volterra formulation (27), together with the boundary identities above, the fractional minimum principle, and uniqueness, excludes a first crossing of either coordinate through zero. Hence

$$X(t) \geq 0, \qquad Y(t) \geq 0, \qquad t \geq 0. \tag{33}$$

Hence,

$$(X(t), Y(t)) \in \mathbb{R}^2_{\geq 0} \quad \forall t \geq 0. \tag{34}$$

(iii) *Global boundedness.* Set $\overline{X} = \max\{X_0, K\}$. The scalar comparison principle gives $0 \leq X(t) \leq \overline{X}$, because the prey component is non-positive at $X = \overline{X}$. Define $V = kX + Y$, $G_{\max} = \max_{0\leq x\leq \overline{X}}\left[rx(1 - x/K)(x/A-1)\right]_+$, and $C = kG_{\max} + dk\overline{X}$. Cancellation of the predation terms yields ${}^{\mathrm{C}}D_t^\alpha V \leq C - dV$. Therefore,

$$0 \leq V(t) \leq V(0)E_\alpha(-dt^\alpha) + \frac{C}{d}\left[1 - E_\alpha(-dt^\alpha)\right], \tag{35}$$

which bounds $X(t) \leq V(t)/k$ and $Y(t) \leq V(t)$ uniformly.

Step 5. Global continuation.

Since the solution remains in a bounded positive region B, where $\mathcal{F}$ is Lipschitz with constant L_B, the continuation theorem for fractional Volterra systems ensures global existence:

$$U(t) \in C([0,\infty), B) \subset C([0,\infty), \mathbb{R}^2_{\geq 0}). \tag{36}$$

Therefore, the model is globally well–posed. □

4.2. Invariant region and boundedness

Lemma 2 (Positively invariant bounded region)**.** *For the fractional predator–prey model* (21)–(22) *with parameters* $r, K, A, k, d, m, b, c > 0$, $\varepsilon \geq 0$, *and* $0 < \alpha \leq 1$, *there exists a compact absorbing set*

$$\Omega = \{(\mathcal{X}, \mathcal{Y}) \in \mathbb{R}^2_+ : \ 0 \leq \mathcal{X} \leq \overline{X}, \ k\mathcal{X} + \mathcal{Y} \leq M\}, \tag{37}$$

where $\overline{X} = \max\{\mathcal{X}_0, K\}$ *and* $M > 0$, *such that:*

1. *Every solution starting in* Ω *remains inside* Ω *for all* $t \geq 0$;
2. *Every nonnegative trajectory is bounded and eventually remains in such a set; this boundedness alone does not select its asymptotic equilibrium.*

Sketch of Proof. We evaluate the vector field of (21)–(22) along the boundary of (37).

(a) *Left boundary* $\mathcal{X} = 0$. From (21), ${}^{C}D^{\alpha}_{t}\mathcal{X} = 0 \Rightarrow \mathcal{X}(t) \geq 0$.

(b) *Right boundary* $\mathcal{X} = \overline{X}$.

$${}^{C}D^{\alpha}_{t}\mathcal{X}\big|_{\mathcal{X}=\overline{X}} \leq -m\overline{X}\mathcal{Y} \leq 0, \tag{38}$$

because $\overline{X} \geq K$, so the prey component points inward.

(c) *Bottom boundary* $\mathcal{Y} = 0$.

$${}^{C}D^{\alpha}_{t}\mathcal{Y} = 0 \Rightarrow \mathcal{Y}(t) \geq 0. \tag{39}$$

(d) *Weighted boundary* $k\mathcal{X} + \mathcal{Y} = M$.

$${}^{C}D^{\alpha}_{t}(k\mathcal{X} + \mathcal{Y}) \leq C - d(k\mathcal{X} + \mathcal{Y}), \tag{40}$$

where $C = kG_{\max} + dk\overline{X}$ is defined above. An inward condition holds whenever

$$M \geq \max\left\{k\mathcal{X}_0 + \mathcal{Y}_0, \frac{C}{d}\right\} \quad \Longrightarrow \quad {}^{C}D^{\alpha}_{t}(k\mathcal{X} + \mathcal{Y}) \leq 0. \tag{41}$$

Conclusion. Conditions (38)–(41), fractional comparison, and quasipositivity imply that Ω is positively invariant and absorbing. They establish boundedness but do not imply convergence to a prescribed attractor [22,23,32]. □

4.3. Numerical scheme and convergence verification

The two model equations are numerically solved via the fractional Adams–Bashforth–Moulton predictor–corrector (ABM–PC) method (cf. [31,46]). To check reliability and numerical consistency, simulations are performed under successive time steps h, and the corresponding global maximum errors E_h are computed against a refined solution with $h_{\text{ref}} = 0.003125$. The experimental convergence order of the ABM–PC method is evaluated by

$$p = \frac{\log(E_{h_1}/E_{h_2})}{\log(h_1/h_2)}, \tag{42}$$

where E_{h_i} denotes the numerical error at step size h_i. A rate $p \approx \min\{2, 1+\alpha\}$ is expected under the regularity assumptions of the predictor–corrector method, and Table 2 confirms this behaviour.

Table 2. Convergence study of the fractional Adams–Bashforth–Moulton (ABM–PC) scheme for Eq. (**??**) to (**??**) at $\alpha = 0.9$ with parameters $r = 1.0$, $K = 8.0$, $A = 1.2$, $m = 0.5$, $k = 0.8$, $d = 0.3$, $b = 0.2$, $c = 0.1$, $\varepsilon = 0.1$

h (step size)	*Max. error in* $\mathcal{X}(t)$	*Max. error in* $\mathcal{Y}(t)$	*p (observed order)*
0.10	3.8514×10^{-2}	5.8472×10^{-2}	—
0.05	1.0638×10^{-2}	1.5532×10^{-2}	1.91
0.025	2.8668×10^{-3}	4.1462×10^{-3}	1.90
0.0125	7.3781×10^{-4}	1.0635×10^{-3}	1.96

The observed orders in Table 2 cluster around the theoretical $1+\alpha = 1.9$ rate. At $\alpha = 1$ and $h = 0.025$, comparison with a DOP853 reference solution gives maximum errors 2.86×10^{-4} in $\mathcal{X}$ and 3.41×10^{-4} in $\mathcal{Y}$, providing an independent implementation check consistent with the ABM–PC analysis [31,46].

5. Nullclines, isoclines and equilibria

Definition 5 (Nullclines & isoclines in the fractional system)**.** Consider the fractional predator–prey model

$$ {}^{C}D_t^{\alpha}\mathcal{X} = f_1(\mathcal{X},\mathcal{Y}), \qquad {}^{C}D_t^{\alpha}\mathcal{Y} = f_2(\mathcal{X},\mathcal{Y}), \qquad 0 < \alpha \le 1, $$

where, from equations (21)–(22),

$$ f_1 = r\mathcal{X}\Big(1-\tfrac{\mathcal{X}}{K}\Big)\Big(\tfrac{\mathcal{X}}{A}-1\Big) - \Phi(\mathcal{X})\mathcal{Y}, \qquad f_2 = k\Phi(\mathcal{X})\mathcal{Y} - d\mathcal{Y} - \varepsilon F(\mathcal{Y})\mathcal{X}, $$

with interaction terms

$$ \Phi(\mathcal{X}) = m\mathcal{X}, \qquad F(\mathcal{Y}) = \frac{b\mathcal{Y}}{1+c\mathcal{Y}}. $$

(i) *Fractional Nullclines.* Equilibria satisfy

$$ {}^{C}D_t^{\alpha}\mathcal{X} = 0, \qquad {}^{C}D_t^{\alpha}\mathcal{Y} = 0 \quad \Longleftrightarrow \quad f_1 = 0,\ f_2 = 0, $$

(hence nullclines are independent of α). Explicitly,

$$ m\mathcal{Y} = r\Big(1-\frac{\mathcal{X}}{K}\Big)\Big(\frac{\mathcal{X}}{A}-1\Big), \qquad km\mathcal{X} - d = \varepsilon\frac{b\mathcal{X}}{1+c\mathcal{Y}}. $$

Thus an equilibrium satisfies

$$ E^* = (\mathcal{X}^*,\mathcal{Y}^*) \in \mathcal{N}_{\mathcal{X}} \cap \mathcal{N}_{\mathcal{Y}}, $$

where position is independent of α, but stability varies strongly with α.

(ii) *Fractional isoclines.* For $\alpha = 1$ the phase-plane slope equals the vector-field ratio below. For $0 < \alpha < 1$, no local chain rule identifies this ratio with $d\mathcal{Y}/d\mathcal{X}$; we therefore use it only as an instantaneous vector-field diagnostic:

$$ \psi(\mathcal{X},\mathcal{Y}) = \frac{f_2(\mathcal{X},\mathcal{Y})}{f_1(\mathcal{X},\mathcal{Y})} = \psi \quad \Longleftrightarrow \quad \mathcal{I}_{\psi} = \{\, f_2 - \psi f_1 = 0 \,\}. $$

Special cases:

$$ \psi = 0 \Rightarrow \mathcal{N}_{\mathcal{Y}}, \qquad \psi \to \infty \Rightarrow \mathcal{N}_{\mathcal{X}}. $$

Lemma 3 (Nullclines and isoclines in Caputo fractional systems)**.** *Let $0 < \alpha \le 1$ and consider the autonomous fractional system*

$$ \begin{cases} {}^{C}D_t^{\alpha}\mathcal{X}(t) = f_1(\mathcal{X}(t),\mathcal{Y}(t)), \\ {}^{C}D_t^{\alpha}\mathcal{Y}(t) = f_2(\mathcal{X}(t),\mathcal{Y}(t)), \end{cases} \qquad (\mathcal{X},\mathcal{Y}) \in \mathbb{R}^2, \tag{43} $$

where f_1, f_2 are continuous and locally Lipschitz (see [22,23,31]*).*

Then the following hold:

1. *Equilibria. A point $(\mathcal{X}^*,\mathcal{Y}^*)$ is an equilibrium of* (43) *iff*

$$ f_1(\mathcal{X}^*,\mathcal{Y}^*) = 0, \qquad f_2(\mathcal{X}^*,\mathcal{Y}^*) = 0. $$

   Hence, the equilibrium set is identical to the integer-order system .
2. *Fractional vector-field ratio. For solutions with ${}^{C}D_t^{\alpha}\mathcal{X}(t) \neq 0$,*

$$ \frac{{}^{C}D_t^{\alpha}\mathcal{Y}(t)}{{}^{C}D_t^{\alpha}\mathcal{X}(t)} = \frac{f_2(\mathcal{X}(t),\mathcal{Y}(t))}{f_1(\mathcal{X}(t),\mathcal{Y}(t))}, \tag{44} $$

so $(\mathcal{X}, \mathcal{Y})$ *lies on the diagnostic level set* $\mathcal{I}_\psi$ *iff*

$$^{C}D_t^{\alpha}\mathcal{Y} = \psi\, {}^{C}D_t^{\alpha}\mathcal{X}.$$

3. *Nullclines as limiting diagnostic sets. The nullclines are limiting vector-field-ratio sets:*

$$\mathcal{N}_{\mathcal{Y}} = \mathcal{I}_0, \qquad \mathcal{N}_{\mathcal{X}} = \mathcal{I}_\infty,$$

and their intersection yields all equilibria of (43).
4. *Memory interpretation* $(0 < \alpha < 1)$*. Although relation* (44) *is algebraically valid, it is not the tangent slope of a fractional trajectory. From the Caputo kernel,*

$$^{C}D_t^{\alpha}\mathcal{X}(t) = \frac{1}{\Gamma(1-\alpha)}\int_0^t \frac{\dot{\mathcal{X}}(\tau)}{(t-\tau)^{\alpha}}d\tau, \tag{45}$$

the ordinary derivatives that determine the plotted trajectory depend on the full history and cannot be recovered from the state-space ratio alone. Thus, nullcline–isocline diagrams identify equilibria and compare the two vector-field components, but do not specify fractional phase tangents or the full temporal evolution [9,32].

Sketch of Proof. Statements (i)–(iii) follow from the definitions of equilibria, nullclines, and the algebraic ratio of the right-hand sides. Dividing the two fractional equations in (43) yields (44), but this operation does not invoke an ordinary chain rule. Statement (iv) follows from the nonlocal Caputo representation (45): the history-dependent ordinary tangent is not determined solely by the current vector-field ratio. Thus, the diagnostic geometry remains algebraically identical to the classical case, while the temporal parametrisation is memory dependent for $0 < \alpha < 1$. Existence and uniqueness of the fractional trajectory are guaranteed by local Lipschitz continuity together with the well-posedness theorem (Theorem 2; cf. [22,23,31]). □

Lemma 4 (Nullclines and interior equilibrium of the proposed PP model)**.** *Consider the fractional predator–prey system* (21) -(22) *with interaction terms* (20)*. For* $\mathcal{X} > 0$*, the prey and predator nullclines are :*

$$\mathcal{N}_{\mathcal{X}} : r\left(1 - \frac{\mathcal{X}}{K}\right)\left(\frac{\mathcal{X}}{A} - 1\right) = m\,\mathcal{Y}, \tag{46}$$

$$\mathcal{N}_{\mathcal{Y}} : km\,\mathcal{X} - d = \varepsilon\,\frac{b\,\mathcal{X}}{1 + c\,\mathcal{Y}}, \tag{47}$$

(cf. Definition 5). Any coexistence equilibrium $E^* = (\mathcal{X}^*, \mathcal{Y}^*)$ *must satisfy*

$$E^* \in \mathcal{N}_{\mathcal{X}} \cap \mathcal{N}_{\mathcal{Y}}.$$

For $\varepsilon > 0$*, eliminating* $\mathcal{Y}$ *from* (46)–(47) *yields the scalar equation for* $\mathcal{X}^*$*:*

$$\frac{r}{m}\left(1 - \frac{\mathcal{X}^*}{K}\right)\left(\frac{\mathcal{X}^*}{A} - 1\right) = \frac{1}{c}\left(\frac{\varepsilon b\,\mathcal{X}^*}{km\mathcal{X}^* - d} - 1\right), \tag{48}$$

and once $\mathcal{X}^*$ *is obtained,*

$$\mathcal{Y}^* = \frac{r}{m}\left(1 - \frac{\mathcal{X}^*}{K}\right)\left(\frac{\mathcal{X}^*}{A} - 1\right). \tag{49}$$

A biologically feasible interior equilibrium exists iff

$$\mathcal{X}^* \in (A, K), \qquad \mathcal{Y}^* > 0, \qquad km\mathcal{X}^* - d > 0, \tag{50}$$

ensuring that (48) *is well defined and positive. When* $\varepsilon = 0$*, the predator nullcline instead reduces to* $km\mathcal{X}^* - d = 0$ *and must be handled without division.*

Proof. At equilibrium, the Caputo derivatives in system (20) vanish, hence

$$0 = r\mathcal{X}\left(1-\frac{\mathcal{X}}{K}\right)\left(\frac{\mathcal{X}}{A}-1\right) - \Phi(\mathcal{X})\mathcal{Y}.$$

For $\mathcal{X} > 0$ and using $\Phi(\mathcal{X}) = m\mathcal{X}$ from equation (20), division by $\mathcal{X}$ yields (46) the prey-nullcline. Similarly,

$$0 = k\,\Phi(\mathcal{X})\mathcal{Y} - d\,\mathcal{Y} - \varepsilon\,F(\mathcal{Y})\mathcal{X},$$

and with $F(\mathcal{Y}) = \dfrac{b\mathcal{Y}}{1+c\mathcal{Y}}$ we obtain (47), the predator-nullcline.

Eliminating $\mathcal{Y}$ by substituting

$$\mathcal{Y} = \frac{r}{m}\left(1-\frac{\mathcal{X}}{K}\right)\left(\frac{\mathcal{X}}{A}-1\right),$$

(from (46)) into the predator nullcline (47) gives the scalar equilibrium Eq. (48). Evaluating (46) at $\mathcal{X} = \mathcal{X}^*$ then yields (49). Positivity of the prey-nullcline expression requires $A < \mathcal{X}^* < K$ and $\mathcal{Y}^* > 0$, while for $\varepsilon > 0$ $km\mathcal{X}^* - d > 0$ keeps (48) nonsingular and positive. These conditions lead to feasibility requirement (50). □

Lemma 5 (Scalar equilibrium equation and cubic form)**.** *For the fractional predator–prey system 20 with* $\Phi(\mathcal{X}) = m\mathcal{X}$ *and* $F(\mathcal{Y}) = \dfrac{b\mathcal{Y}}{1+c\mathcal{Y}}$ *eliminating* $\mathcal{Y}$ *from the nullcline relations yields*

$$c(km\mathcal{X}-d)\,\frac{r}{m}\left(1-\frac{\mathcal{X}}{K}\right)\left(\frac{\mathcal{X}}{A}-1\right) - \Big[\mathcal{X}(\varepsilon b - km) + d\Big] = 0. \tag{51}$$

This relation defines all interior equilibria $\mathcal{X}^* > 0$ *of the system.*
After expansion, (51) *reduces to the cubic*

$$P(\mathcal{X}) = \mathsf{a}_3\mathcal{X}^3 + \mathsf{a}_2\mathcal{X}^2 + \mathsf{a}_1\mathcal{X} + \mathsf{a}_0 = 0, \tag{52}$$

where, with $S = A^{-1} + K^{-1}$, *the coefficients depend algebraically on* $(r, K, A, k, d, m, b, c, \varepsilon)$ *and are:*

$$\mathsf{a}_3 = \frac{cr(km)}{mKA}, \mathsf{a}_2 = -\frac{cr}{m}\left(kmS + \frac{d}{AK}\right), \mathsf{a}_1 = \frac{cr}{m}(km + dS) + \varepsilon b - km, \mathsf{a}_0 = d\left(1-\frac{cr}{m}\right). \tag{53}$$

Each positive real root $\mathcal{X}^*$ *gives a unique predator density*

$$\mathcal{Y}^* = \frac{r}{m}\left(1-\frac{\mathcal{X}^*}{K}\right)\left(\frac{\mathcal{X}^*}{A}-1\right) = \frac{\mathcal{X}^*(\varepsilon b - km) + d}{c(km\mathcal{X}^* - d)},$$

hence each feasible root determines one coexistence equilibrium, subject to

$$\mathcal{X}^* \in (A, K), \quad \mathcal{Y}^* > 0, \quad km\mathcal{X}^* - d > 0.$$

The prey nullcline is strictly concave on (A, K), *whereas the predator nullcline is decreasing and convex for* $\mathcal{X} > d/(km)$ *when* $\varepsilon > 0$. *Their difference is strictly concave, so at most two of the cubic roots can be biologically feasible.*

Lemma 6 (Equilibrium set and maximal number of equilibria)**.** *Consider system* (20) *with parameters* $r, K, A, k, d, m, b, c > 0$, $\varepsilon \geq 0$ *and* $0 < A < K$, *and interaction functions* $\Phi(\mathcal{X}) = m\mathcal{X}$, $F(\mathcal{Y}) = \dfrac{b\mathcal{Y}}{1+c\mathcal{Y}}$ *(cf.* (20)*). Then:*

1. *Boundary equilibria. The system always admits three boundary equilibria:*

$$E_0 = (0,0), \qquad E_A = (A,0), \qquad E_K = (K,0), \tag{54}$$

corresponding respectively to total extinction, Allee-threshold prey equilibrium, and prey saturation at carrying capacity.

2. *Interior (coexistence) equilibria. Any coexistence equilibrium $E^* = (\mathcal{X}^*, \mathcal{Y}^*)$ with $\mathcal{X}^* > 0$, $\mathcal{Y}^* > 0$ satisfies the cubic scalar equation (52) from Lemma 5. Hence, the prey density $\mathcal{X}^*$ is a positive real root of the cubic polynomial $P(\mathcal{X})$ and the associated predator density is given by*

$$\mathcal{Y}^* = \frac{r}{m}\left(1 - \frac{\mathcal{X}^*}{K}\right)\left(\frac{\mathcal{X}^*}{A} - 1\right) = \frac{\mathcal{X}^*(\varepsilon b - km) + d}{c(km\mathcal{X}^* - d)}. \tag{55}$$

3. *Maximum number of equilibria. The cubic $P(\mathcal{X})$ admits at most three distinct real roots. Consequently, the number of biologically feasible coexistence equilibria*

$$N_{\text{coex}} := \#\{\mathcal{X}^* \in (A, K) : \ P(\mathcal{X}^*) = 0, \ \mathcal{Y}^* > 0, \ km\mathcal{X}^* - d > 0\},$$

satisfies

$$0 \le N_{\text{coex}} \le 2.$$

Therefore, the total number of biologically feasible equilibria is bounded by

$$3 \le N_{\text{eq}} = 3 + N_{\text{coex}} \le 5. \tag{56}$$

Lemma 7 (Discriminant of the equilibrium cubic)**.** *For the scalar equilibrium cubic polynomial $P(\mathcal{X})$ (52) the discriminant for polynomial (52) is given by*

$$\Delta = 18\mathsf{a}_3\mathsf{a}_2\mathsf{a}_1\mathsf{a}_0 - 4\mathsf{a}_2^3\mathsf{a}_0 + \mathsf{a}_2^2\mathsf{a}_1^2 - 4\mathsf{a}_3\mathsf{a}_1^3 - 27\mathsf{a}_3^2\mathsf{a}_0^2, \tag{57}$$

Remark 1 (On the number of real roots)**.** In principle, the sign of the discriminant (57) determines the number of real roots of the cubic polynomial $P(\mathcal{X})$: $\Delta > 0$ corresponds to three distinct real roots, $\Delta = 0$ to multiple (real) roots, and $\Delta < 0$ to exactly one real root and a complex-conjugate pair (cf. Lemma 1). However, the explicit expression for Δ in (57) depends in a highly nonlinear way on the parameters $(r, K, A, k, d, m, b, c, \varepsilon)$, so its sign cannot be characterized by a simple closed-form condition. Therefore, in this model the actual number of real (and biologically feasible) equilibria must be determined by numerical evaluation of Δ and by direct computation of the roots of $P(\mathcal{X})$ for specific parameter sets.

Lemma 8 (Critical points and qualitative shape of the equilibrium cubic)**.** *Let*

$$P(\mathcal{X}) = \mathsf{a}_3\mathcal{X}^3 + \mathsf{a}_2\mathcal{X}^2 + \mathsf{a}_1\mathcal{X} + \mathsf{a}_0, \qquad \mathsf{a}_3 \neq 0.$$

Then

$$P'(\mathcal{X}) = 3\mathsf{a}_3\mathcal{X}^2 + 2\mathsf{a}_2\mathcal{X} + \mathsf{a}_1. \tag{58}$$

The critical (extreme) points are the real solutions of $P'(\mathcal{X}) = 0$, i.e.

$$\mathcal{X}_\pm = \frac{-2\mathsf{a}_2 \pm \sqrt{4\mathsf{a}_2^2 - 12\mathsf{a}_3\mathsf{a}_1}}{6\mathsf{a}_3} = \frac{-\mathsf{a}_2 \pm \sqrt{\mathsf{a}_2^2 - 3\mathsf{a}_3\mathsf{a}_1}}{3\mathsf{a}_3}, \tag{59}$$

whenever the discriminant

$$\Delta_1 := \mathsf{a}_2^2 - 3\mathsf{a}_3\mathsf{a}_1, \tag{60}$$

is nonnegative.

(i) *If $\Delta_1 < 0$, then $P'(\mathcal{X})$ has no real zeros, so P is strictly monotone on $\mathbb{R}$ and thus has exactly one real root.*
(ii) *If $\Delta_1 = 0$, then $P'(\mathcal{X})$ has one real double root*

$$\mathcal{X}_c = -\frac{\mathsf{a}_2}{3\mathsf{a}_3},$$

and P has an inflection point with horizontal tangent at $\mathcal{X} = \mathcal{X}_c$. In this case P has either a triple real root or a simple root plus a double root.

(iii) *If $\Delta_1 > 0$, then $P'(\mathcal{X})$ has two distinct real roots $\mathcal{X}_- < \mathcal{X}_+$, given by (59), and P has one local maximum and one local minimum. The number of real roots of P is then determined by the signs of*

$$P(\mathcal{X}_-), \qquad P(\mathcal{X}_+):$$

if $P(\mathcal{X}_-) > 0$ and $P(\mathcal{X}_+) > 0$ (or both < 0), there is exactly one real root; if $P(\mathcal{X}_-) > 0 > P(\mathcal{X}_+)$ (or the opposite), P has three distinct real roots.

Lemma 9 (Critical points and root structure of the equilibrium for our model)**.** *Consider the fractional predator–prey model with interaction terms $\Phi(\mathcal{X}) = m\mathcal{X}$ and $F(\mathcal{Y}) = \dfrac{b\mathcal{Y}}{1+c\mathcal{Y}}$. Writing $S = A^{-1} + K^{-1}$, the coexistence equilibrium $\mathcal{X}^*$ is determined by the cubic polynomial*

$$P(\mathcal{X}) = \underbrace{\frac{crkm}{mKA}}_{\mathsf{a}_3}\mathcal{X}^3 + \underbrace{-\frac{cr}{m}\left(kmS + \frac{d}{AK}\right)}_{\mathsf{a}_2}\mathcal{X}^2 + \underbrace{\left[\frac{cr}{m}(km + dS) + \varepsilon b - km\right]}_{\mathsf{a}_1}\mathcal{X} + \underbrace{d\left(1 - \frac{cr}{m}\right)}_{\mathsf{a}_0} = 0. \tag{61}$$

The derivative of $P(\mathcal{X})$ is

$$P'(\mathcal{X}) = 3\frac{crkm}{mKA}\mathcal{X}^2 - 2\frac{cr}{m}\left(kmS + \frac{d}{AK}\right)\mathcal{X} + \frac{cr}{m}\left[km + d\left(\frac{1}{A} + \frac{1}{K}\right)\right] + \varepsilon b - km. \tag{62}$$

Define the discriminant-like quantity

$$\Delta_1 = \mathsf{a}_2^2 - 3\mathsf{a}_3\mathsf{a}_1. \tag{63}$$

Substituting the coefficients $\mathsf{a}_3, \mathsf{a}_2, \mathsf{a}_1$ into (63) yields:

$$\Delta_1 = \left[\frac{cr}{m}\left(km\left(\frac{1}{A} + \frac{1}{K}\right) + \frac{d}{AK}\right)\right]^2 - 3\left(\frac{crkm}{mKA}\right)\left[\frac{cr}{m}(km + dS) + \varepsilon b - km\right]. \tag{64}$$

The sign of Δ_1 determines the stationary points and the real-root structure of the cubic $P(\mathcal{X})$:

- *If $\Delta_1 < 0$, then $P(\mathcal{X})$ is monotonic and the equation*

$$P(\mathcal{X}) = 0, \tag{65}$$

has exactly one real root.
- *If $\Delta_1 = 0$, then $P(\mathcal{X})$ has a repeated stationary point, and the cubic admits either one or two distinct real roots.*
- *If $\Delta_1 > 0$, then $P(\mathcal{X})$ has two turning points located at*

$$X_\pm = \frac{-\mathsf{a}_2 \pm \sqrt{\Delta_1}}{3\mathsf{a}_3} = \frac{\frac{cr}{m}\left[km\left(\frac{1}{A} + \frac{1}{K}\right) + \frac{d}{AK}\right] \pm \sqrt{\Delta_1}}{3\frac{crkm}{mKA}}. \tag{66}$$

The cubic possesses three distinct real roots if and only if

$$P(X_-)\,P(X_+) < 0. \tag{67}$$

Otherwise, it has exactly one real root.

Biologically feasible coexistence requires

$$\mathcal{X}^* \in (A, K), \qquad \mathcal{Y}^* > 0, \qquad km\,\mathcal{X}^* > d, \tag{68}$$

which implies that multiple coexistence equilibria may exist, but only those satisfying (68) are ecologically admissible.

Remark 2 (On the actual number of coexistence equilibria)**.** In principle, the number of real roots of the equilibrium cubic $P(\mathcal{X})$ can be characterized by two complementary analytic tools:

(i) the *discriminant* Δ of $P(\mathcal{X})$ (Lemma 7), which determines whether the cubic has one or three real roots in $\mathbb{R}$; and
(ii) the *critical point* analysis via $P'(\mathcal{X})$ (Lemma 8), which uses the turning points $X_\pm$ and the signs of $P(X_\pm)$ to distinguish between one and three real roots.

However, for the present model the corresponding expressions $\Delta = \Delta(r, K, A, k, d, m, b, c, \varepsilon)$ and $\Delta_1 = \Delta_1(r, K, A, k, d, m, b, c, \varepsilon)$ depend on the parameters in a highly nonlinear way. As a consequence, neither approach yields a simple closed-form condition on $(r, K, A, k, d, m, b, c, \varepsilon)$ that would *a priori* fix the exact number of real (and biologically feasible) coexistence equilibria.

Therefore, in this work the classification of equilibria and the detection of parameter regimes with one or multiple coexistence states are carried out *numerically*, by evaluating the roots of $P(\mathcal{X})$ and checking the feasibility conditions

$$\mathcal{X}^* > 0, \qquad \mathcal{Y}^* > 0, \qquad km\mathcal{X}^* > d,$$

for each parameter set considered in the simulations.

6. Local stability and hopf bifurcation analysis

Lemma 10 (Jacobian matrix)**.** *The Jacobian $\mathcal{J}(\mathcal{X}, \mathcal{Y}) = D\mathcal{F}(\mathcal{X}, \mathcal{Y})$ of the fractional predator–prey model is*

$$\mathcal{J}(\mathcal{X}, \mathcal{Y}) = \begin{pmatrix} \partial_{\mathcal{X}} f_1 & \partial_{\mathcal{Y}} f_1 \\ \partial_{\mathcal{X}} f_2 & \partial_{\mathcal{Y}} f_2 \end{pmatrix}, \tag{69}$$

with entries

$$\partial_{\mathcal{X}} f_1(\mathcal{X}, \mathcal{Y}) = r\left(\frac{2\mathcal{X}}{A} + \frac{2\mathcal{X}}{K} - 1 - \frac{3\mathcal{X}^2}{AK}\right) - m\mathcal{Y}, \tag{70}$$

$$\partial_{\mathcal{Y}} f_1(\mathcal{X}, \mathcal{Y}) = -m\mathcal{X}, \tag{71}$$

$$\partial_{\mathcal{X}} f_2(\mathcal{X}, \mathcal{Y}) = km\mathcal{Y} - \varepsilon \frac{b\mathcal{Y}}{1 + c\mathcal{Y}}, \tag{72}$$

$$\partial_{\mathcal{Y}} f_2(\mathcal{X}, \mathcal{Y}) = km\mathcal{X} - d - \varepsilon \frac{b\mathcal{X}}{(1 + c\mathcal{Y})^2}. \tag{73}$$

In particular, $\mathcal{J}$ does not depend on the fractional order α; only the stability region in the complex plane changes with α.

Lemma 11 (Jacobian and stability at boundary equilibria)**.** *Consider the fractional predator–prey model (21)–(22) with Jacobian $\mathcal{J}(\mathcal{X}, \mathcal{Y})$ given in Lemma 10. Let*

$$E_0 = (0, 0), \qquad E_A = (A, 0), \qquad E_K = (K, 0),$$

denote the trivial and prey-only equilibria. Then:

(i) *Trivial equilibrium $E_0 = (0, 0)$:*

$$\mathcal{J}(E_0) = \begin{pmatrix} -r & 0 \\ 0 & -d \end{pmatrix}, \qquad \lambda_1 = -r, \quad \lambda_2 = -d.$$

Since $r, d > 0$, both eigenvalues are real and negative. Hence E_0 is a hyperbolic asymptotically stable node for $\alpha = 1$, and, by the Matignon criterion $|\arg(\lambda_i)| > \frac{\alpha\pi}{2}$, it remains locally asymptotically stable for all $0 < \alpha < 1$.

(ii) *Prey-only equilibrium at the Allee threshold $E_A = (A, 0)$:*

$$\mathcal{J}(E_A) = \begin{pmatrix} r\left(1 - \frac{A}{K}\right) & -mA \\ 0 & A(km - \varepsilon b) - d \end{pmatrix},$$

with eigenvalues

$$\lambda_1 = r\left(1 - \frac{A}{K}\right), \qquad \lambda_2 = A(km - \varepsilon b) - d.$$

Equivalently,

$$\lambda_1 < 0 \iff A > K, \qquad \lambda_2 < 0 \iff km < \varepsilon b + \frac{d}{A}.$$

Thus

$$\begin{cases} \text{Stable node}, & A > K \text{ and } km < \varepsilon b + \dfrac{d}{A}, \\ \text{Saddle}, & (K - A)\left(A(km - \varepsilon b) - d\right) < 0, \\ \text{Unstable node}, & A < K \text{ and } km > \varepsilon b + \dfrac{d}{A}. \end{cases}$$

In particular, under the biological assumption $0 < A < K$, one has $\lambda_1 > 0$, so E_A is always unstable (a saddle if $\lambda_2 < 0$ and an unstable node if $\lambda_2 > 0$). Because this positive real eigenvalue violates Matignon's criterion for every α, fractional order cannot stabilise E_A.

(iii) *Prey-only equilibrium at carrying capacity $E_K = (K, 0)$:*

$$\mathcal{J}(E_K) = \begin{pmatrix} r\left(1 - \dfrac{K}{A}\right) & -mK \\ 0 & K(km - \varepsilon b) - d \end{pmatrix},$$

with eigenvalues

$$\lambda_1 = r\left(1 - \frac{K}{A}\right), \qquad \lambda_2 = K(km - \varepsilon b) - d.$$

Hence

$$\lambda_1 < 0 \iff K > A, \qquad \lambda_2 < 0 \iff km < \varepsilon b + \frac{d}{K},$$

and

$$\begin{cases} \text{Stable node}, & K > A \text{ and } km < \varepsilon b + \dfrac{d}{K}, \\ \text{Saddle}, & (A - K)\left(K(km - \varepsilon b) - d\right) < 0, \\ \text{Unstable node}, & K < A \text{ and } km > \varepsilon b + \dfrac{d}{K}. \end{cases}$$

Since $0 < A < K$, one has $\lambda_1 < 0$, so the sign of λ_2 is controlled by the balance between predation strength km and anti-predator feedback plus mortality $\varepsilon b + d/K$. Thus E_K is stable for every $0 < \alpha \leq 1$ when $\lambda_2 < 0$ and is a saddle for every order when $\lambda_2 > 0$.

Lemma 12 (Jacobian and local stability at the coexistence equilibrium). *Let $\mathcal{X}^* > 0$ be a positive root of the scalar cubic equilibrium equation $P(\mathcal{X}) = 0$, and let*

$$\mathcal{Y}^* = \frac{r}{m}\left(1 - \frac{\mathcal{X}^*}{K}\right)\left(\frac{\mathcal{X}^*}{A} - 1\right) = \frac{\mathcal{X}^*(\varepsilon b - km) + d}{c(km\mathcal{X}^* - d)},$$

be the corresponding predator density (cf. Lemma 4). Assume the feasibility conditions

$$\mathcal{X}^* \in (A, K), \qquad \mathcal{Y}^* > 0, \qquad km\mathcal{X}^* - d > 0,$$

hold, so that

$$E^* = (\mathcal{X}^*, \mathcal{Y}^*),$$

is a biologically meaningful coexistence equilibrium. Then the Jacobian of system (20) at E^* is

$$\mathcal{J}(E^*) = \begin{pmatrix} J_{11}^* & J_{12}^* \\ J_{21}^* & J_{22}^* \end{pmatrix}, \tag{74}$$

where, using Lemma 10,

$$J_{11}^* = r\left(\frac{2\mathcal{X}^*}{A} + \frac{2\mathcal{X}^*}{K} - 1 - \frac{3(\mathcal{X}^*)^2}{AK}\right) - m\mathcal{Y}^*, \tag{75}$$

$$J_{12}^* = -m\mathcal{X}^*, \tag{76}$$

$$J_{21}^* = km\mathcal{Y}^* - \varepsilon\frac{b\mathcal{Y}^*}{1+c\mathcal{Y}^*}, \tag{77}$$

$$J_{22}^* = km\mathcal{X}^* - d - \varepsilon\frac{b\mathcal{X}^*}{(1+c\mathcal{Y}^*)^2}. \tag{78}$$

Let

$$\tau^* = \operatorname{tr}\mathcal{J}(E^*) = J_{11}^* + J_{22}^*, \qquad \Delta^* = \det\mathcal{J}(E^*) = J_{11}^*J_{22}^* - J_{12}^*J_{21}^*,$$

so that the characteristic polynomial is

$$\lambda^2 - \tau^*\lambda + \Delta^* = 0.$$

Then:

- *for $\alpha = 1$ (classical ODE), E^* is locally asymptotically stable if*

$$\tau^* < 0, \qquad \Delta^* > 0;$$

- *for $0 < \alpha < 1$ (fractional Caputo system), E^* is locally asymptotically stable if and only if both eigenvalues $\lambda_{1,2} \in \mathbb{C}$ of $\mathcal{J}(E^*)$ satisfy the Matignon condition*

$$\left|\arg(\lambda_i)\right| > \frac{\alpha\pi}{2}, \qquad i = 1,2.$$

Remark 3 (Stability depends on the cubic root; numerical evaluation required)**.** The quantities $(\mathcal{X}^*, \mathcal{Y}^*, \tau^*, \Delta^*)$ depend nonlinearly on the cubic equilibrium root and the model parameters. Hence no closed-form stability condition is analytically tractable. Therefore, the stability of E^* is assessed *numerically*, by computing $\mathcal{X}^*$ from $P(\mathcal{X})$, generating E^*, and evaluating (τ^*, Δ^*) and $\lambda_{1,2}$ for given parameter sets.

6.1. Limit cycle and Hopf bifurcation analysis

Lemma 13 (Hopf bifurcation at the coexistence equilibrium)**.** *Let $E^* = (\mathcal{X}^*, \mathcal{Y}^*)$ be the positive coexistence equilibrium generated by the cubic condition. Let τ^* and Δ^* be the trace and determinant of $\mathcal{J}(E^*)$ as defined in Lemma 12, and let μ be a bifurcation parameter taken from $\mu \in \{r, K, A, k, d, m, b, c, \varepsilon\}$.*

For the integer-order system $\alpha = 1$, a nondegenerate Hopf bifurcation is possible at $\mu = \mu_c$ only if the following local conditions hold:

$$\tau^*(\mu_c) = 0, \tag{79}$$

$$\Delta^*(\mu_c) > 0, \tag{80}$$

$$\left.\frac{d\tau^*}{d\mu}\right|_{\mu=\mu_c} \neq 0. \tag{81}$$

Stability change:

$$\begin{aligned} \tau^*(\mu) < 0,\ \Delta^* > 0 \quad &\Rightarrow \quad E^* \text{ stable}, \\ \tau^*(\mu) > 0,\ \Delta^* > 0 \quad &\Rightarrow \quad E^* \text{ unstable}. \end{aligned}$$

Fractional case: If $0 < \alpha < 1$, *the corresponding local stability-sector boundary is*

$$\left|\arg(\lambda_{1,2}(\mu_c))\right| = \frac{\alpha\pi}{2},$$

so that complex eigenvalues leave the Matignon stability sector. This is a fractional stability transition, not by itself a Hopf bifurcation. Autonomous Caputo systems of non-integer order do not admit exact nonconstant periodic solutions, although oscillatory transients may occur (cf. [21,32,39]).

Remark 4 (Practical implication for this model)**.** Because τ^* and Δ^* depend nonlinearly on the cubic equilibrium root $\mathcal{X}^*$, candidate crossings are located numerically by computing $P(\mathcal{X})$, evaluating τ^*, Δ^*, and checking feasibility and transversality. Only the $\alpha = 1$ crossing can be interpreted as a classical Hopf candidate; for $0 < \alpha < 1$ the reported boundary has the narrower meaning of a Matignon-sector stability transition.

Remark 5 (Ecological interpretation)**.** A classical Hopf-generated limit cycle at $\alpha = 1$ represents sustained predator–prey oscillations: prey density increases first, predators grow with delay, and the resulting predation pressure drives the prey back down, completing the cycle. For $0 < \alpha < 1$, exact periodic solutions are excluded, while the Caputo memory term can alter oscillatory transients and convergence rates. Such memory dependence can represent ecological effects such as delayed reproduction, gradual predation response, or resource regeneration lag ([8,9,11,32]).

Lemma 14 (Basin-restricted Mittag–Leffler stability of the coexistence equilibrium)**.** *Assume that the fractional predator–prey system* (21)–(22) *admits a biologically feasible interior equilibrium* $E^* = (\mathcal{X}^*, \mathcal{Y}^*)$, *with*

$$\mathcal{X}^* \in (A, K), \qquad \mathcal{Y}^* > 0, \qquad km\mathcal{X}^* - d > 0. \tag{82}$$

Let $\Omega_* \subset \mathbb{R}^2_{>0}$ *be a compact positively invariant set containing* E^* *in its interior and no other equilibrium. Define*

$$g(\mathcal{X}) := r\,\mathcal{X}\Big(1 - \frac{\mathcal{X}}{K}\Big)\Big(\frac{\mathcal{X}}{A} - 1\Big), \qquad g'(\mathcal{X}) = -\frac{r}{AK}\big(AK - 2(A+K)\mathcal{X} + 3\mathcal{X}^2\big), \tag{83}$$

and the local prey-curvature scalar

$$\Phi_1(\mathcal{X}^*) := -\frac{m}{r}\,g'(\mathcal{X}^*) = \frac{m}{AK}\Big(AK - 2(A+K)\mathcal{X}^* + 3(\mathcal{X}^*)^2\Big). \tag{84}$$

The screening condition

$$\Phi_1(\mathcal{X}^*) > 0, \tag{85}$$

is useful but is not, by itself, a global dissipation condition. For $\gamma > 0$, *define*

$$\Gamma_{\min}(\Omega_*) := \inf\Big\{\gamma > 0 :\ \exists\,\eta > 0 \ \text{ with } \ \mathcal{R}_\gamma \le -\eta\big[(\mathcal{X} - \mathcal{X}^*)^2 + (\mathcal{Y} - \mathcal{Y}^*)^2\big] \ \text{ on } \ \Omega_*\Big\}. \tag{86}$$

Here $\mathcal{R}_\gamma$ *is the exact expression specified in the proof. If this defining set is nonempty, choose any admissible* γ *from that defining set and consider the Volterra-type logarithmic Lyapunov functional*

$$V(\mathcal{X}, \mathcal{Y}) = \mathcal{X}^*\Big(\frac{\mathcal{X}}{\mathcal{X}^*} - 1 - \ln\frac{\mathcal{X}}{\mathcal{X}^*}\Big) + \gamma\,\mathcal{Y}^*\Big(\frac{\mathcal{Y}}{\mathcal{Y}^*} - 1 - \ln\frac{\mathcal{Y}}{\mathcal{Y}^*}\Big). \tag{87}$$

Then, along any solution $(\mathcal{X}(t), \mathcal{Y}(t))$ *of* (21)–(22) *remaining in* Ω_*, *one has*

$${}^{\mathrm{C}}D_t^{\alpha} V(\mathcal{X}(t), \mathcal{Y}(t)) \le 0, \qquad t \ge 0, \tag{88}$$

with equality if and only if $(\mathcal{X}(t), \mathcal{Y}(t)) = E^*$. *Moreover, V is positive definite and coercive on* Ω_*. *Consequently, the fractional Lyapunov theorem gives asymptotic Mittag–Leffler stability relative to* Ω_*. *This conclusion cannot be extended to the whole positive quadrant because* E_0 *is locally asymptotically stable for every* $0 < \alpha \le 1$.

Proof. *Step 1: Positivity and coercivity of V.* For $u > 0$ the function $\phi(u) := u - 1 - \ln u$, is strictly convex, $\phi(u) \geq 0$, and $\phi(u) = 0$ iff $u = 1$. Therefore each term in (87) is nonnegative and

$$V(\mathcal{X}, \mathcal{Y}) \geq 0, \qquad V(\mathcal{X}, \mathcal{Y}) = 0 \iff (\mathcal{X}, \mathcal{Y}) = (\mathcal{X}^*, \mathcal{Y}^*).$$

Moreover, $\phi(u) \to \infty$ as $u \to 0^+$ or $u \to \infty$. On the compact set Ω_*, V is therefore coercive and has the unique minimum $V(E^*) = 0$.

Step 2: Fractional chain rule inequality. By Lemma 2.1 of Li and Chen [31] the Caputo derivative of $\phi(\mathcal{X}/\mathcal{X}^*)$ satisfies

$${}^{\mathrm{C}}D_t^{\alpha}\phi\Big(\frac{\mathcal{X}}{\mathcal{X}^*}\Big) \leq \Big(1 - \frac{\mathcal{X}^*}{\mathcal{X}}\Big)\,{}^{\mathrm{C}}D_t^{\alpha}\mathcal{X},$$

and similarly for $\mathcal{Y}$. Multiplying by $\mathcal{X}^*$ and $\gamma\mathcal{Y}^*$ yields

$${}^{\mathrm{C}}D_t^{\alpha}V \leq \Big(1 - \frac{\mathcal{X}^*}{\mathcal{X}}\Big)\,{}^{\mathrm{C}}D_t^{\alpha}\mathcal{X} + \gamma\Big(1 - \frac{\mathcal{Y}^*}{\mathcal{Y}}\Big)\,{}^{\mathrm{C}}D_t^{\alpha}\mathcal{Y}. \tag{89}$$

Step 3: Exact dissipation expression. Substitute the dynamics (21)–(22) into (89). With

$$g(\mathcal{X}^*) = m\mathcal{X}^*\mathcal{Y}^*, \qquad km\mathcal{X}^*\mathcal{Y}^* = d\mathcal{Y}^* + \varepsilon\frac{b\mathcal{Y}^*}{1 + c\mathcal{Y}^*}\mathcal{X}^*.$$

the resulting upper bound is

$${}^{\mathrm{C}}D_t^{\alpha}V \leq \mathcal{R}_{\gamma}(\mathcal{X}, \mathcal{Y}) \leq -\eta\left[(\mathcal{X} - \mathcal{X}^*)^2 + (\mathcal{Y} - \mathcal{Y}^*)^2\right], \tag{90}$$

where

$$\mathcal{R}_{\gamma} = \Big(1 - \frac{\mathcal{X}^*}{\mathcal{X}}\Big)f_1(\mathcal{X}, \mathcal{Y}) + \gamma\Big(1 - \frac{\mathcal{Y}^*}{\mathcal{Y}}\Big)f_2(\mathcal{X}, \mathcal{Y}).$$

The second inequality is precisely the stated verifiable condition; it must be checked on the selected invariant set and is not implied by equilibrium identities alone.

Step 4: Select an admissible weight. For any admissible γ in the defining set of (86), compactness gives

$$\mathcal{R}_{\gamma}(\mathcal{X}, \mathcal{Y}) \leq -\eta\|(\mathcal{X}, \mathcal{Y}) - E^*\|^2,$$

for some $\eta > 0$. Then

$${}^{\mathrm{C}}D_t^{\alpha}V \leq 0,$$

with equality only at $(\mathcal{X}, \mathcal{Y}) = E^*$.

Step 5: Apply the fractional Lyapunov theorem. Since Ω_* is compact and positively invariant, (88) implies convergence of trajectories in this certified set to E^*. Hence the coexistence equilibrium is Mittag–Leffler stable relative to Ω_*. The open basin of the stable extinction equilibrium excludes global coexistence attraction in $\mathbb{R}^2_{>0}$. □

7. Results and discussion

7.1. Complete solution and graphical representation of the system

The fractional-order predator–prey model was integrated with the Diethelm–Ford–Freed predictor–corrector (ABM–PC) scheme (cf. [46]) for several orders $0 < \alpha \leq 1$. Unless stated otherwise, the initial state is $\mathcal{X}(0) = 3.0$, $\mathcal{Y}(0) = 0.5$. The three simulation groups use, respectively, $t \in [0, 20]$ with $h = 0.025$, $t = 15$ with $h = 0.05$, and $t \in [0, 30]$ with $h = 0.025$.

Figure 3 displays the temporal trajectories and phase portraits for $\alpha = 0.2$, 0.4, 0.6, 0.8, and 1.0, with parameter values $r = 1.0$, $K = 10.0$, $A = 2.0$, $m = 0.5$, $k = 0.8$, $d = 0.3$, $b = 0.2$, $c = 0.1$, $\varepsilon = 0.1$. For this parameter set the corrected cubic has no feasible coexistence equilibrium; the trajectories instead approach the stable extinction state E_0. At $t = 20$, the computed states change from $(1.1870, 0.7902)$ at $\alpha = 0.2$ to $(1.30 \times 10^{-7}, 0.01276)$ at $\alpha = 1$. Thus, decreasing α substantially slows the observed decline and retains both populations over the finite observation window, but it does not create a new equilibrium or remove the

extinction basin. The predator peaks increase from 1.0201 to 2.1272 as α increases from 0.2 to 1, while the contour and surface panels show the corresponding history-dependent relaxation ([22,32]).

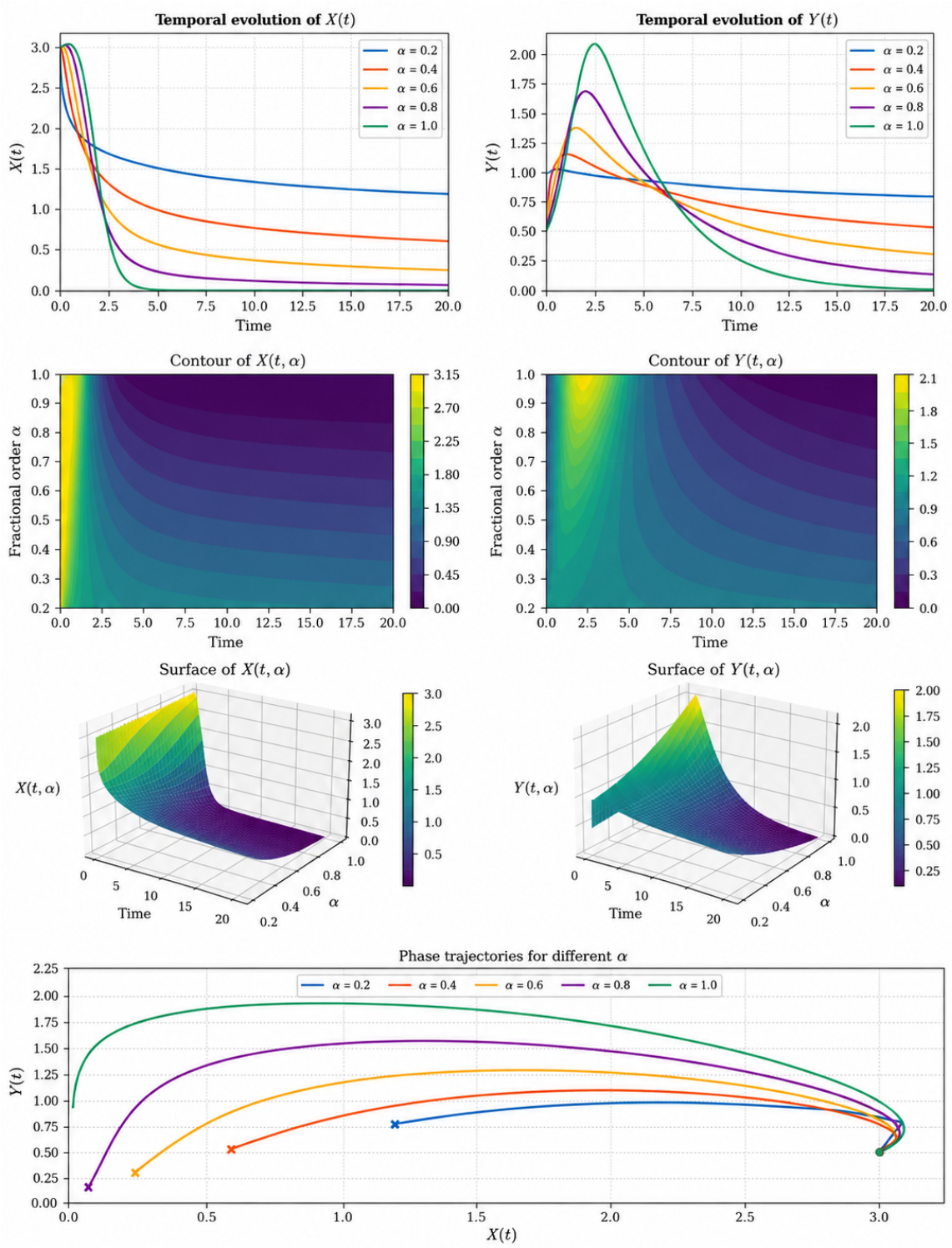

Figure 3. Temporal evolution and phase portraits of the fractional predator–prey model for fractional orders $\alpha = \{1.0, 0.8, 0.6, 0.4, 0.2\}$ with initial condition $(\mathcal{X}(0), \mathcal{Y}(0)) = (3.0, 0.5)$. Parameters used are $r = 1.0$, $K = 10.0$, $A = 2.0$, $m = 0.5$, $k = 0.8$, $d = 0.3$, $b = 0.2$, $c = 0.1$, $\varepsilon = 0.1$. Smaller fractional order $(\alpha < 1)$ generates slower relaxation, reduced oscillation amplitude, and longer transient persistence, whereas the classical case $(\alpha = 1)$ converges rapidly with sharper predator–prey cycles. The 3D surfaces highlight how decreasing α smooths trajectories and increases recovery time, confirming the memory–driven damping predicted by fractional stability theory. This figure clearly demonstrates how ecological memory alters oscillations, coexistence duration, and equilibrium convergence

Figure 4 further examines the interplay between the fractional order α, the Allee threshold A, and carrying capacity K. Simulations were performed for $A \in \{1.3, 1.8, 2.3\}$ and $\alpha \in \{0.7, 0.86, 0.9, 1.0\}$ with other parameters fixed. These are finite-time values rather than equilibria. At fractional orders 0.7–0.9, increasing K reduces the small residual prey density but increases the predator density at $t = 15$; for example, at $\alpha = 0.9$ and $A = 1.3$, $\mathcal{Y}(15)$ rises from 0.2315 at $K = 6$ to 0.5771 at $K = 16$. Increasing A lowers the predator remnant throughout the scan. The $\alpha = 1$ prey values are already near zero, whereas smaller α retains a larger transient population. Accordingly, the sweep quantifies delayed decline rather than asymptotic coexistence.

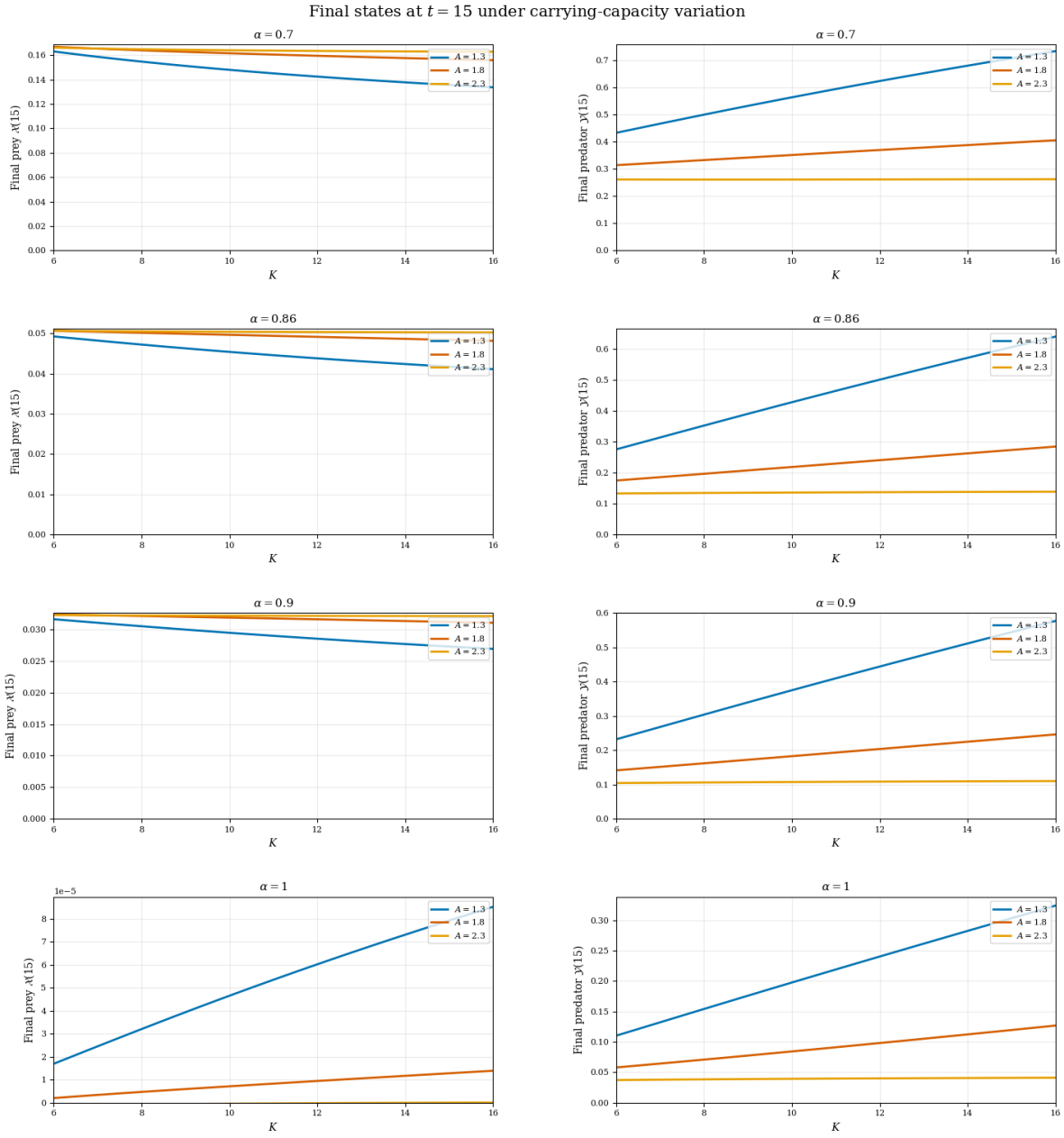

Figure 4. Variation of final prey density $\mathcal{X}(15)$ (left column) and predator density $\mathcal{Y}(15)$ (right column) with carrying capacity K for four fractional orders $\alpha = \{0.7, 0.86, 0.9, 1.0\}$ and three Allee thresholds $A = \{1.3, 1.8, 2.3\}$. Smaller Allee thresholds support higher prey survival, while larger A reduces both populations through stronger Allee suppression. Predator density initially increases with K due to enhanced prey availability, but eventually declines once prey becomes scarce at high K. Lower fractional order $\alpha < 1$ produces smoother convergence and slower decay, indicating memory–driven persistence, whereas the classical model ($\alpha = 1$) responds rapidly and stabilizes faster. This figure highlights the combined regulatory roles of memory (α), carrying capacity (K), and Allee threshold (A) in determining long–term coexistence stability

Figure 5 resolves the transient time series. At $A = 1.2$, the states at $t = 30$ are $(0.1861, 0.3107)$, $(0.04668, 0.13595)$, and $(1.94 \times 10^{-7}, 0.00236)$ for $\alpha = 0.6$, 0.8, and 1, respectively. The classical trajectory also has the largest predator peak (10.1061), compared with 4.8758 for $\alpha = 0.6$. In the fixed-order scan $\alpha = 0.9$, increasing A from 0.8 to 1.6 lowers the predator peak from 12.2143 to 4.3435 and the predator value at $t = 30$ from 0.07596 to 0.04019. These results support a finite-time memory effect: smaller α lengthens the transient, while stronger Allee pressure reduces predator support; neither observation alone establishes asymptotic coexistence [23,32].

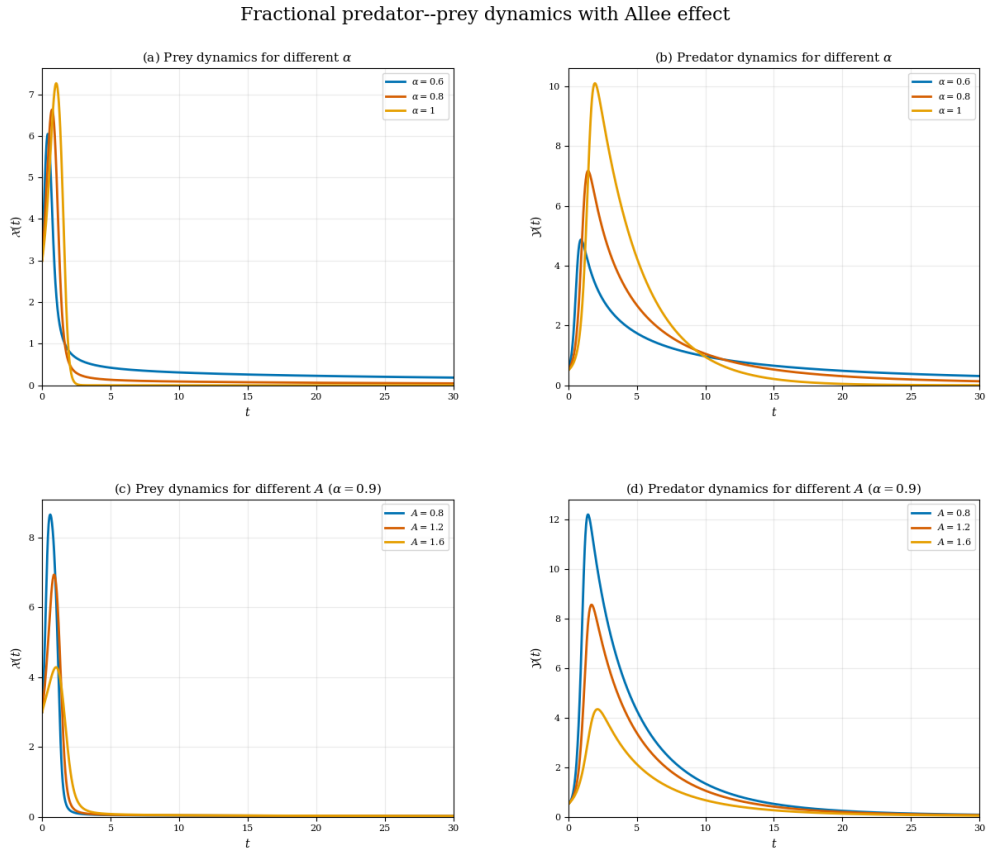

Figure 5. Transient prey–predator dynamics under variation of fractional order α (top row) and Allee threshold A (bottom row). Panels (a)–(b) show the effect of fractional memory $\alpha = \{0.6, 0.8, 1.0\}$ with fixed $A = 1.2$, revealing that smaller $\alpha < 1$ yields slower convergence, damped oscillations, and prolonged coexistence, whereas the classical case $\alpha = 1$ settles rapidly with higher predator peaks. Panels (c)–(d) illustrate the impact of Allee intensity $A = \{0.8, 1.2, 1.6\}$ under fixed fractional dynamics $\alpha = 0.9$: larger A weakens prey recovery and suppresses predator density, increasing extinction risk. The comparison demonstrates how fractional memory buffers Allee collapse by slowing transients and extending coexistence. Parameters used: $r = 1.0$, $K = 10.0$, $m = 0.5$, $k = 0.8$, $d = 0.3$, $b = 0.2$, $c = 0.1$, $\varepsilon = 0.1$, with initial condition $(\mathcal{X}(0), \mathcal{Y}(0)) = (3, 0.5)$

The surfaces in Figure 6 use the same ABM–PC implementation to separate the effects of fractional order and conversion efficiency. The top row confirms that smaller α retains larger residual populations over $t \leq 30$. In the k sweeps, increasing conversion efficiency raises the predator response and accelerates prey depletion for both $\alpha = 1$ and $\alpha = 0.9$. The fractional and classical surfaces should therefore be read as different transient time parametrisations, not as evidence that α changes the nullclines or equilibrium locations [36].

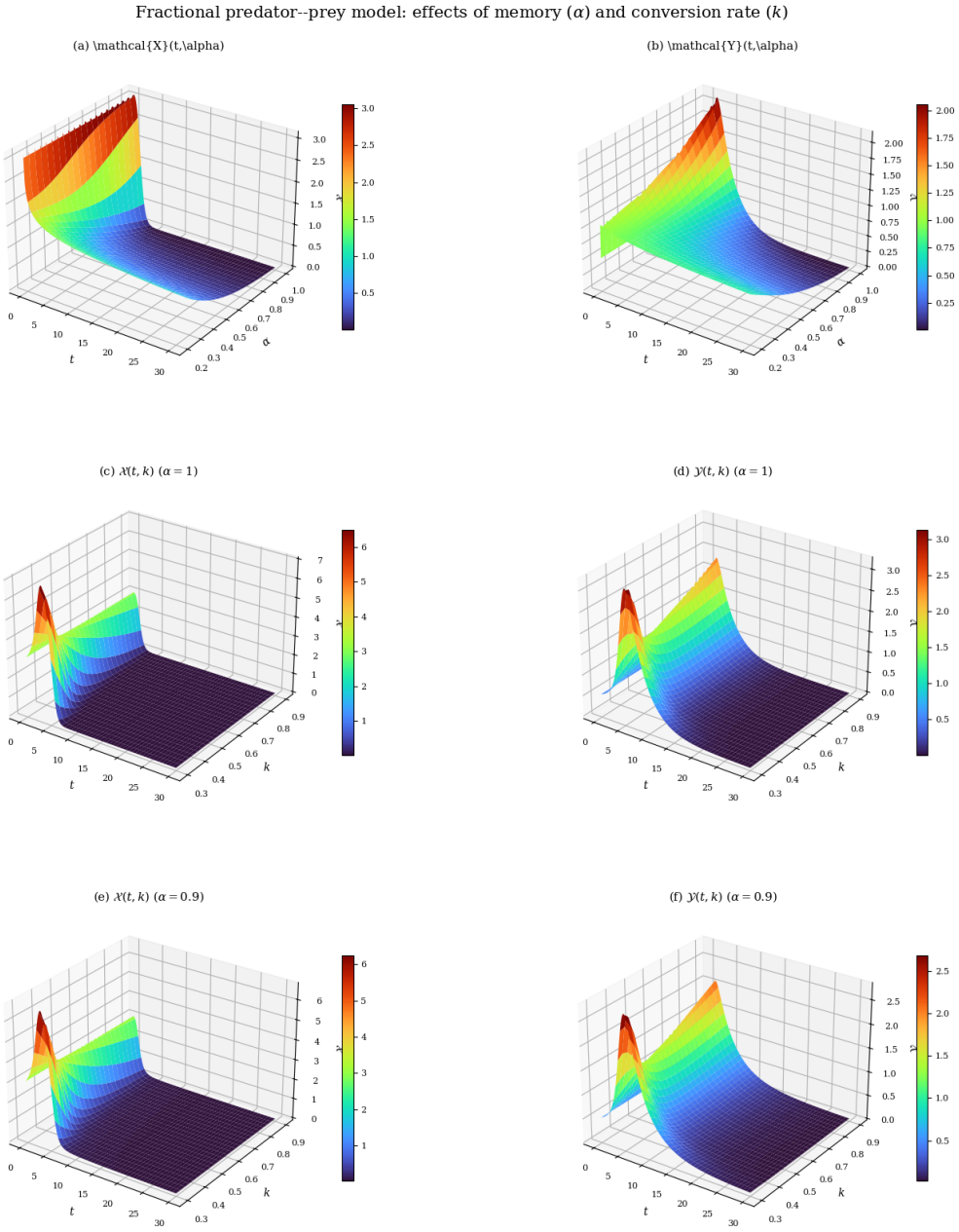

Figure 6. Surface evolution of prey $\mathcal{X}(t,\cdot)$ and predator $\mathcal{Y}(t,\cdot)$ densities under joint variation of the fractional order α and conversion efficiency k, with initial condition $(\mathcal{X}(0),\mathcal{Y}(0)) = (3, 0.5)$. *Top row (a–b):* Variation in α ($0.2 \leq \alpha \leq 1$) shows that smaller fractional order introduces strong memory effects, producing slow relaxation, reduced amplitude, and prolonged coexistence. *Middle row (c–d):* Classical system ($\alpha = 1$) where increasing k markedly increases oscillatory overshoot in predator growth and accelerates prey decline. *Bottom row (e–f):* Fractional regime ($\alpha = 0.9$) where increasing k still boosts predator density, but memory smooths transients and suppresses peaks, yielding faster stabilization compared to $\alpha = 1$. Overall, the figure illustrates how fractional memory moderates conversion-driven instability and delays predator–prey collapse

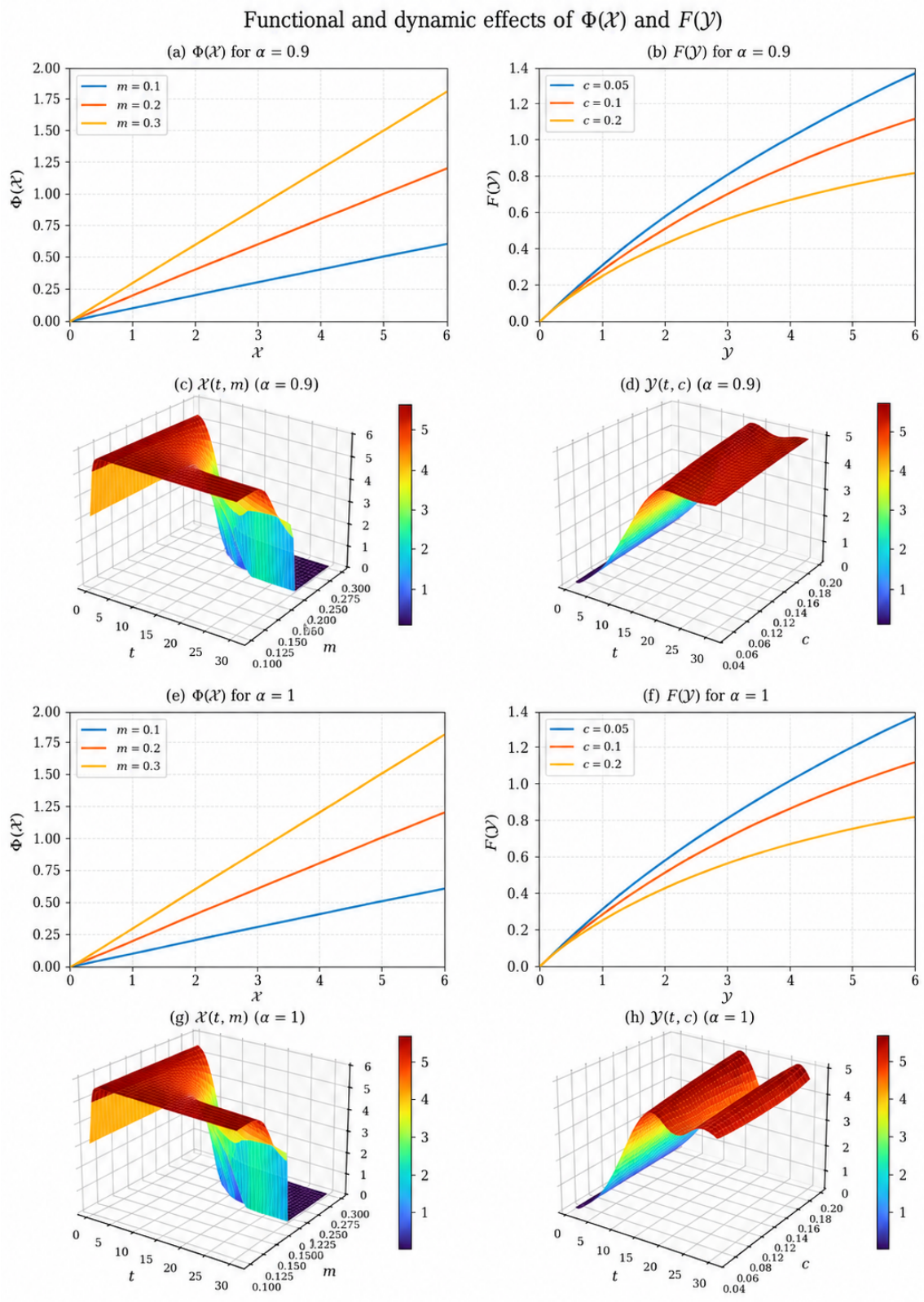

Figure 7. *Functional and dynamic effects of the predation term* $\Phi(\mathcal{X}) = m\mathcal{X}$ *and anti–predator defence* $F(\mathcal{Y}) = \frac{b\mathcal{Y}}{1+c\mathcal{Y}}$ *for fractional* ($\alpha = 0.9$) *and classical* ($\alpha = 1.0$) *dynamics.* Panels (a–b) and (e–f) show how increasing m intensifies linear predation, while increasing c saturates defence response and reduces predator efficiency. Panels (c–d) and (g–h) display the corresponding time–evolution surfaces $\mathcal{X}(t, m)$ and $\mathcal{Y}(t, c)$ under $\alpha = 0.9$ and $\alpha = 1.0$. Fractional order ($0 < \alpha < 1$) yields smoother trajectories, weaker oscillatory peaks and slow recovery, indicating memory-driven consumption and extended coexistence. In contrast, $\alpha = 1$ responds instantaneously and produces sharper fluctuations and faster turnover. Overall, fractional memory lowers oscillation energy, delays predator escalation and enhances long-term population persistence.

7.2. Impact of predation and feedback responses under fractional and classical dynamics

A comparative analysis of the nonlinear interaction functions $\Phi(\mathcal{X}) = m\mathcal{X}$ (prey–dependent predation rate) and $F(\mathcal{Y}) = \frac{b\mathcal{Y}}{1+c\mathcal{Y}}$ (saturating anti–predator feedback) is presented in Figure 7 for both fractional ($\alpha = 0.9$) and classical ($\alpha = 1.0$) dynamics. The parameter settings used are $r = 1.2$, $K = 6.0$, $A = 1.2$, $m = 0.2$, $k = 0.6$, $d = 0.4$, $\varepsilon = 0.05$, $b = 0.3$, $c = 0.1$, for which the corrected equilibrium is $E^* = (3.6409, 4.7986)$ with eigenvalues -0.01882 ± 0.61882 i at $K = 6$ and $A = 1.2$. These values provide a controlled setting for observing how α, m, and c alter transient population behaviour (cf. [32,36]). Increasing m steepens $\Phi(\mathcal{X}) = m\mathcal{X}$ exactly and, in the dynamic surfaces, intensifies prey removal. The $\alpha = 0.9$ and $\alpha = 1$ surfaces have the same equilibria for each parameter value, but different relaxation histories. The feedback loss is governed by $F(\mathcal{Y}) = \frac{b\mathcal{Y}}{1+c\mathcal{Y}}$, where small c is nearly linear, whereas larger c lowers the magnitude of $F(\mathcal{Y})$ at a fixed predator density. Because this term enters the predator equation with a minus sign, increasing c weakens the anti-predator loss; it must not be interpreted as reduced predator efficiency. The line plots verify these monotonic functional effects directly, while the surfaces show their nonlinear consequences over a finite time interval ([7,11]). Overall, fractional order changes the temporal response, while m and c also change the vector field and must be assessed through the corrected equilibrium and eigenvalue calculations.

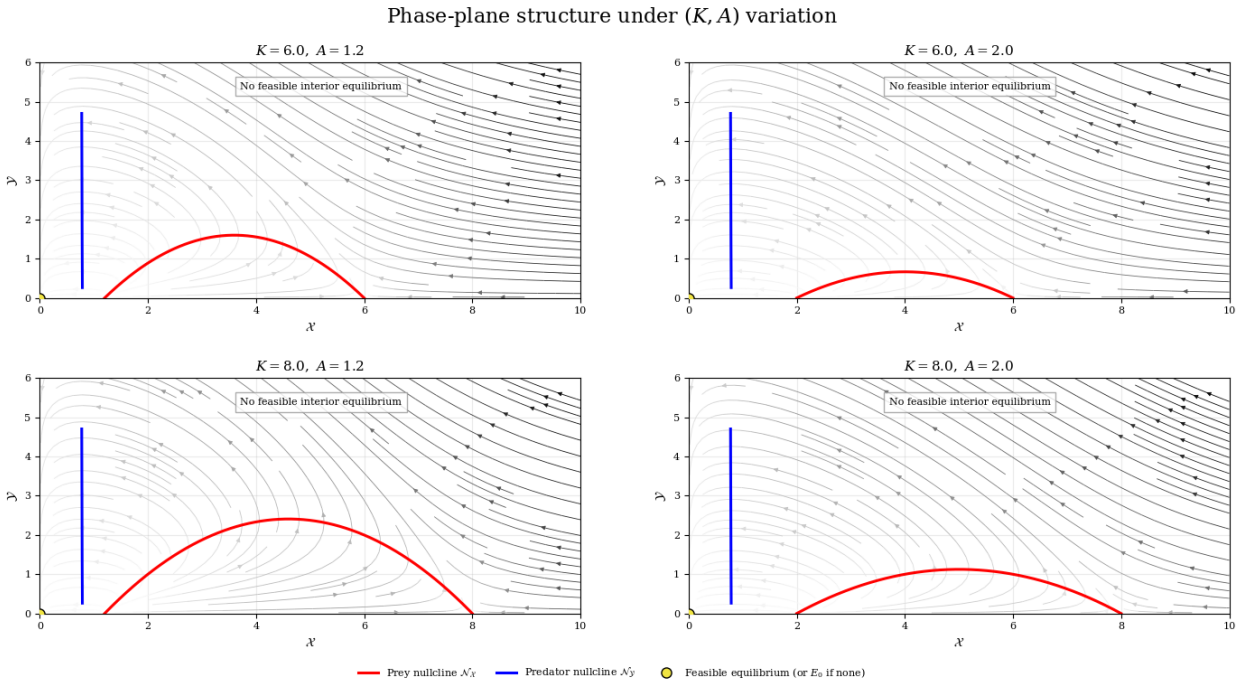

Figure 8. *Phase–plane structure of the predator–prey system under variation of carrying capacity K and Allee threshold A* Each panel shows the vector field together with prey nullcline $\mathcal{N}_\mathcal{X}$ (red), predator nullcline $\mathcal{N}_\mathcal{Y}$ (blue), and equilibrium point $(\mathcal{X}^*, \mathcal{Y}^*)$ (yellow), with parameters $r = 1.0$, $m = 0.5$, $k = 0.8$, $d = 0.3$, $b = 0.2$, $c = 0.1$, $\varepsilon = 0.1$. Increasing K shifts $\mathcal{N}_\mathcal{X}$ rightward, enlarging prey feasibility and increasing predator density at equilibrium. In contrast, higher A elevates the Allee hump, weakening prey recovery and reducing coexistence potential. Across all cases, trajectories spiral or flow toward a single positive equilibrium when persistence occurs, illustrating how (K, A) shape basin geometry, feasibility, and long–term coexistence. This figure quantifies how habitat productivity (K) promotes survival, whereas strong Allee effects (A large) move the system toward collapse.

7.3. Phase-plane structure under carrying-capacity and allee-threshold variation

Figure 8 illustrates the instantaneous vector-field geometry for varying carrying capacities K and Allee thresholds A. Each panel displays $\boldsymbol{\mathcal{F}}(\boldsymbol{\mathcal{U}}) = (f_1, f_2)$ together with the prey and predator nullclines,

$$\mathcal{N}_\mathcal{X} : \; f_1 = 0 \;\Rightarrow\; \mathcal{Y} = \frac{r}{m}\left(1 - \frac{\mathcal{X}}{K}\right)\left(\frac{\mathcal{X}}{A} - 1\right), \qquad \mathcal{N}_\mathcal{Y} : \; f_2 = 0 \;\Rightarrow\; \mathcal{Y} = \frac{1}{c}\left(\frac{\varepsilon b \mathcal{X}}{km\mathcal{X} - d} - 1\right),$$

as defined in Definition 5. The prey nullcline $\mathcal{N}_{\mathcal{X}}$ is a concave hump on (A, K), while $\mathcal{N}_{\mathcal{Y}}$ is a decreasing convex branch on its feasible domain. For the four displayed combinations and the fixed parameters stated in the figure, the branches do not intersect in the positive quadrant. Direct filtering of the corrected cubic confirms $N_{\text{coex}} = 0$ in every panel; the yellow marker therefore denotes E_0, as indicated inside the regenerated figure.

The corrected computations instead give

$$N_{\text{coex}} = 0 \quad \text{for} \quad (K, A) \in \{(6, 1.2), (6, 2.0), (8, 1.2), (8, 2.0)\}.$$

Increasing K widens and raises the prey-nullcline hump, while increasing A shifts its left zero and lowers the hump; neither change is sufficient to create a feasible intersection in this particular slice. This corrected phase geometry prevents a spurious coexistence interpretation and illustrates why algebraic roots must be filtered before stability is discussed [8,9,11,36].

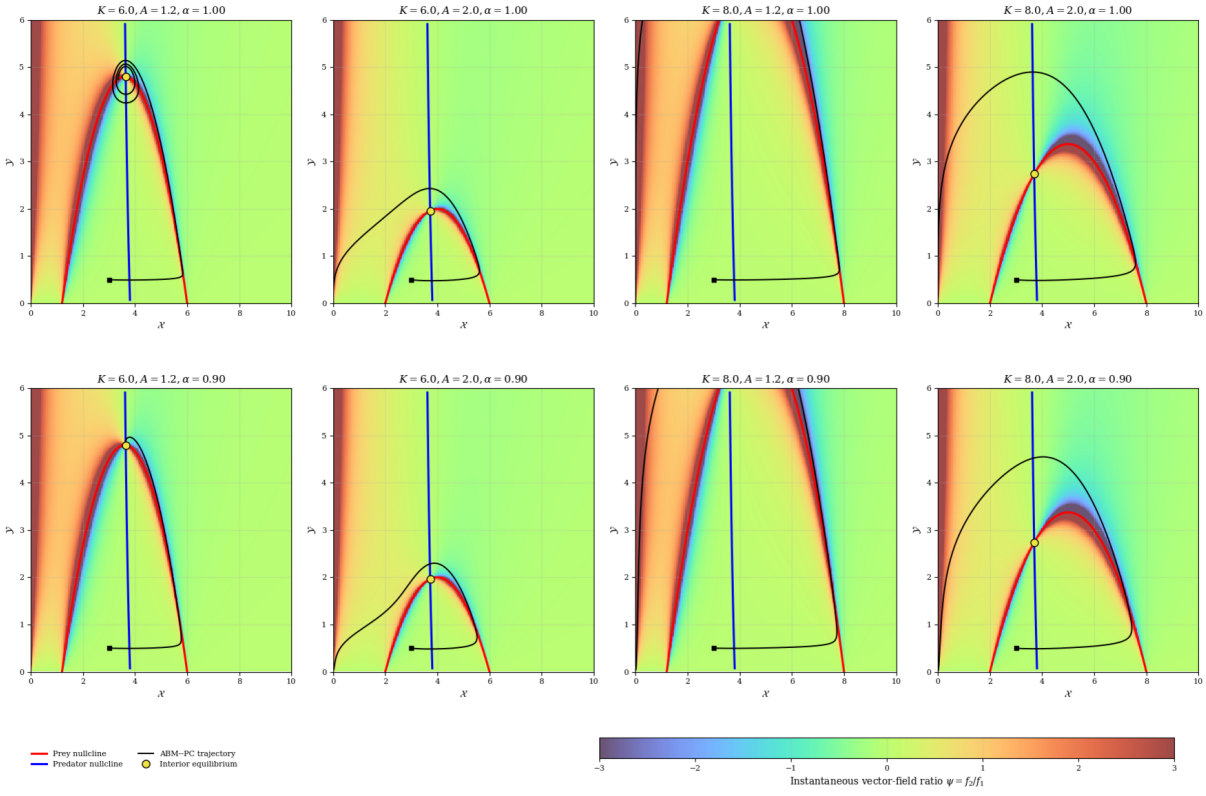

Figure 9. *Classical ($\alpha = 1$) vs fractional ($0 < \alpha < 1$) phase–plane dynamics of the predator–prey system under varying carrying capacity K and Allee threshold A.* Each panel displays vector trajectories, prey/predator nullclines and the interior equilibrium for $(K, A) \in \{(6, 1.2), (6, 2.0), (8, 1.2), (8, 2.0)\}$ with initial populations $(\mathcal{X}(0), \mathcal{Y}(0)) = (3.0, 0.5)$. The top row corresponds to classical integer–order dynamics ($\alpha = 1$), while the bottom row illustrates fractional memory effects with $\alpha = 0.9$. In the classical case, solutions converge rapidly and may generate overshoot oscillations, whereas fractional trajectories approach the equilibrium via slow, damped spirals governed by Mittag–Leffler decay. The memory term delays predator response, smooths prey depletion, and reduces oscillation amplitude. Fractional nonlocality therefore supports coexistence over longer time scales and produces ecologically realistic recovery compared to the sharper classical regime.
Fixed parameters: $r = 1.2$, $m = 0.2$, $k = 0.6$, $d = 0.4$, $b = 0.3$, $c = 0.1$, $\varepsilon = 0.05$.

Figure 9 further compares the phase–plane structure under classical ($\alpha = 1$) and fractional ($0 < \alpha < 1$) dynamics for identical ecological parameters. The background colour is the clipped instantaneous ratio $\psi = f_2/f_1$, not the ordinary phase slope when $\alpha < 1$. At $(K, A) = (6, 1.2)$, the coexistence equilibrium is $(3.6409, 4.7986)$ with eigenvalues -0.01882 ± 0.61882 i and is stable for both displayed orders. For $(6, 2.0)$, $(8, 1.2)$, and $(8, 2.0)$, the corresponding real parts are 0.10719, 0.45495, and 0.36614, respectively; all three

equilibria are unstable for $\alpha = 1$ and $\alpha = 0.9$. The trajectories therefore converge only in the first pair of panels and depart from the interior equilibrium in the other panels. Fractional order changes the transient path and the Matignon threshold, but not the plotted nullclines, equilibrium coordinates, or Jacobian eigenvalues.

7.4. Eigenvalue results and stability analysis

Table 3 summarises, for each value of the carrying capacity K, the discriminant Δ of the cubic equilibrium equation $P(\mathcal{X}) = 0$, the number of real algebraic roots, the number of biologically feasible coexistence states, and the eigenvalue-based stability classification of each feasible equilibrium.

For a cubic with real coefficients, the sign of the discriminant Δ determines the algebraic root structure: $\Delta > 0$ implies three distinct real roots, $\Delta = 0$ a multiple real root, and $\Delta < 0$ exactly one real and two complex conjugate roots. However, not every real root corresponds to a biologically meaningful equilibrium. A coexistence state must satisfy

$$\mathcal{X}^* > 0, \qquad \mathcal{Y}^* = \frac{r}{m}\Big(1 - \frac{\mathcal{X}^*}{K}\Big)\Big(\frac{\mathcal{X}^*}{A} - 1\Big) > 0, \qquad km\,\mathcal{X}^* - d > 0.$$

Therefore, the column "# feasible" in Table 3 counts only those real roots that satisfy all three feasibility conditions. For each feasible root $\mathcal{X}_j^*$, the associated predator density $\mathcal{Y}_j^*$ is computed from the prey nullcline, and the two eigenvalues $\lambda_{1,j}, \lambda_{2,j}$ of the Jacobian $J(E_j^*)$ are evaluated.

All thirteen rows have three real algebraic roots but exactly one feasible root. The feasible equilibrium is a stable focus only at $K = 6$, where $E^* = (3.6409, 4.7986)$ and $\Re(\lambda_{1,2}) = -0.0188$. It becomes an unstable focus at $K = 6.5$ and remains unstable throughout the scan, changing to an unstable node between $K = 10.5$ and $K = 11$. Thus, increased carrying capacity raises the equilibrium predator density but destabilises this particular coexistence branch.

Table 3. Discriminant Δ, real roots of the cubic equilibrium equation $P(\mathcal{X}) = 0$, biologically feasible coexistence equilibria, eigenvalue-based stability, and the effect of carrying capacity K. Fixed parameters: $r = 1.2$, $A = 1.2$, $m = 0.2$, $k = 0.6$, $d = 0.4$, $b = 0.3$, $c = 0.1$, $\varepsilon = 0.05$

K	Δ	*Real*	*Feasible*	*Eq. j*	$\mathcal{X}_j^*$	$\mathcal{Y}_j^*$	$\Re(\lambda_{1,j})$	$\Re(\lambda_{2,j})$	*Stability*
6.0	1.7151×10^{-4}	3	1	1	3.6409	4.7986	-0.0188	-0.0188	Stable
6.5	1.8331×10^{-4}	3	1	1	3.6285	5.3642	0.1298	0.1298	Unstable
7.0	1.9266×10^{-4}	3	1	1	3.6189	5.8418	0.2550	0.2550	Unstable
7.5	2.0016×10^{-4}	3	1	1	3.6111	6.2510	0.3622	0.3622	Unstable
8.0	2.0626×10^{-4}	3	1	1	3.6047	6.6058	0.4550	0.4550	Unstable
8.5	2.1127×10^{-4}	3	1	1	3.5993	6.9166	0.5361	0.5361	Unstable
9.0	2.1543×10^{-4}	3	1	1	3.5947	7.1912	0.6078	0.6078	Unstable
9.5	2.1891×10^{-4}	3	1	1	3.5908	7.4356	0.6715	0.6715	Unstable
10.0	2.2184×10^{-4}	3	1	1	3.5873	7.6546	0.7286	0.7286	Unstable
10.5	2.2433×10^{-4}	3	1	1	3.5843	7.8520	0.7800	0.7800	Unstable
11.0	2.2645×10^{-4}	3	1	1	3.5816	8.0308	0.9647	0.6885	Unstable
11.5	2.2828×10^{-4}	3	1	1	3.5792	8.1937	1.1461	0.5919	Unstable
12.0	2.2985×10^{-4}	3	1	1	3.5771	8.3425	1.2719	0.5436	Unstable

Table 4 reports the complete equilibrium structure generated by a fine–resolution scan of the Allee parameter $A \in [1, 2.6]$ with step 0.05. For each value of A, we compute the cubic equilibrium equation $P(X) = 0$, its discriminant Δ, the total number of real algebraic roots, the number of biologically feasible coexistence equilibria, and the corresponding Jacobian eigenvalues.

Table 4. Equilibrium structure under fine variation of A. For $\Delta > 0$ the cubic has three real roots, but feasibility selects the true eco-equilibria. Only feasible roots yield eigenpairs

A	Δ	Real	Feasible	$\mathcal{X}^*$	$\mathcal{Y}^*$	$\Re(\lambda_1)$	$\Re(\lambda_2)$	Type
1.00	3.50e-04	3	1	3.5743	8.5447	0.5030	0.5030	Unstable
1.05	3.03e-04	3	1	3.5822	7.9906	0.4891	0.4891	Unstable
1.10	2.65e-04	3	1	3.5900	7.4869	0.4766	0.4766	Unstable
1.15	2.33e-04	3	1	3.5974	7.0272	0.4652	0.4652	Unstable
1.20	2.06e-04	3	1	3.6047	6.6058	0.4550	0.4550	Unstable
1.25	1.84e-04	3	1	3.6117	6.2183	0.4456	0.4456	Unstable
1.30	1.65e-04	3	1	3.6185	5.8607	0.4370	0.4370	Unstable
1.35	1.48e-04	3	1	3.6251	5.5297	0.4291	0.4291	Unstable
1.40	1.34e-04	3	1	3.6315	5.2224	0.4219	0.4219	Unstable
1.45	1.22e-04	3	1	3.6378	4.9363	0.4152	0.4152	Unstable
1.50	1.12e-04	3	1	3.6438	4.6694	0.4090	0.4090	Unstable
1.55	1.02e-04	3	1	3.6497	4.4198	0.4033	0.4033	Unstable
1.60	9.42e-05	3	1	3.6554	4.1859	0.3979	0.3979	Unstable
1.65	8.70e-05	3	1	3.6610	3.9662	0.3930	0.3930	Unstable
1.70	8.05e-05	3	1	3.6664	3.7595	0.3884	0.3884	Unstable
1.75	7.48e-05	3	1	3.6717	3.5647	0.3840	0.3840	Unstable
1.80	6.97e-05	3	1	3.6768	3.3808	0.3800	0.3800	Unstable
1.85	6.51e-05	3	1	3.6818	3.2068	0.3762	0.3762	Unstable
1.90	6.09e-05	3	1	3.6867	3.0420	0.3726	0.3726	Unstable
1.95	5.71e-05	3	1	3.6914	2.8858	0.3693	0.3693	Unstable
2.00	5.37e-05	3	1	3.6960	2.7374	0.3661	0.3661	Unstable
2.05	5.06e-05	3	1	3.7006	2.5963	0.3632	0.3632	Unstable
2.10	4.78e-05	3	1	3.7050	2.4619	0.3604	0.3604	Unstable
2.15	4.52e-05	3	1	3.7093	2.3338	0.3577	0.3577	Unstable
2.20	4.28e-05	3	1	3.7134	2.2116	0.3552	0.3552	Unstable
2.25	4.06e-05	3	1	3.7175	2.0949	0.3528	0.3528	Unstable
2.30	3.86e-05	3	1	3.7215	1.9833	0.3506	0.3506	Unstable
2.35	3.67e-05	3	1	3.7254	1.8764	0.3484	0.3484	Unstable
2.40	3.50e-05	3	1	3.7293	1.7740	0.3464	0.3464	Unstable
2.45	3.34e-05	3	1	3.7330	1.6759	0.3444	0.3444	Unstable
2.50	3.19e-05	3	1	3.7366	1.5817	0.3426	0.3426	Unstable
2.55	3.06e-05	3	1	3.7402	1.4912	0.3408	0.3408	Unstable
2.60	2.93e-05	3	1	3.7437	1.4042	0.3392	0.3392	Unstable

- The column Δ represents the discriminant of the cubic. Since $\Delta > 0$ for the entire scan, the cubic *always has three real roots*. This reflects mathematically admissible stationary points, including non-ecological branches.
- The column *Real* lists the count of real algebraic roots returned by the polynomial solver ($= 3$ everywhere, as predicted by $\Delta > 0$).
- The column *Feasible* counts how many of these roots satisfy the ecological viability conditions:

$$X^* \in (A, K), \qquad Y^* > 0, \qquad kmX^* - d > 0.$$

  Only these correspond to biologically meaningful coexistence equilibria.
- In every row of this scan, exactly *one* real root satisfies feasibility, and the remaining two correspond to non-physical states ($Y^* \leq 0$ or predator viability $kmX^* - d < 0$ fails). This parameter slice therefore contains one predator–prey coexistence equilibrium, although the model can admit two feasible intersections in other parameter regimes.
- Columns X^*, Y^* list this surviving equilibrium, and $\Re(\lambda_{1,2})$ give the real parts of eigenvalues of the Jacobian $J(E^*)$. Because both eigenvalues are strictly positive for all A, the coexistence equilibrium is an *unstable focus*; the omitted imaginary parts decrease from 0.6662 at $A = 1$ to 0.0371 at $A = 2.6$.

Despite the cubic producing three real equilibria for every A, ecological constraints reduce this scan to *a single valid coexistence branch*. However, this branch has $\Re(\lambda_1) > 0$ and $\Re(\lambda_2) > 0$ everywhere in the tested

Allee range, implying the predator–prey steady state is *unstable for all* $1 \leq A \leq 2.6$. Increasing A (stronger Allee threshold) lowers predator density and gradually weakens growth feedback, yet instability persists. Fractional stability must be assessed separately from these real parts using Matignon's angular criterion.

7.5. Two–parameter stability maps and Hopf-like bifurcation boundaries

Figure 10 presents four two-parameter maps computed from the corrected cubic and Jacobian, with the remaining quantities fixed at $r = 1.2$, $K = 8$, $A = 1.2$, $m = 0.2$, $k = 0.6$, $d = 0.4$, $b = 0.3$, $c = 0.1$, and $\varepsilon = 0.05$. At every grid point, all real roots were filtered by $\mathcal{X}^* \in (A, K)$, $\mathcal{Y}^* > 0$, and $km\mathcal{X}^* - d > 0$. Gray therefore records the absence of a feasible coexistence state, green a feasible state with negative eigenvalue real parts, and pink a feasible unstable state. In the (A, m) plane, the stable band lies between the lower feasibility boundary and the trace-zero curve; larger m is unstable until feasibility is lost. The (A, K) plane is almost entirely unstable, with a narrow stable segment near $K = 6$. In the (m, K) plane, feasibility first appears as m increases, followed by a stable band and then an unstable region beyond the trace-zero curve. In the (A, ε) plane, stronger feedback shifts the system from instability to stability, and the required ε increases with A. The black curve satisfies $\operatorname{tr} J = 0$ with $\det J > 0$ and complex eigenvalues; it is a classical Hopf candidate only after transversality is checked at $\alpha = 1$, and is not a limit-cycle boundary for $0 < \alpha < 1$.

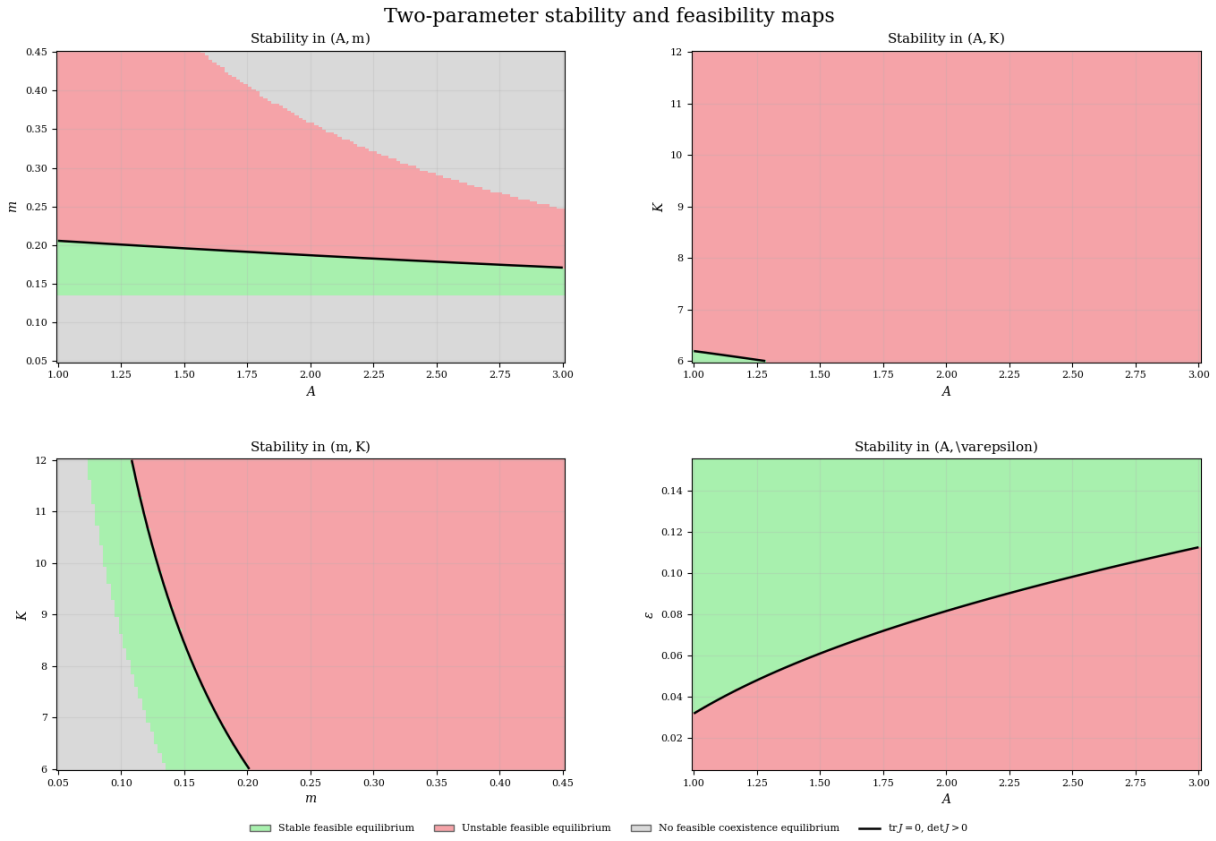

Figure 10. Two–parameter stability maps of the predator–prey system with Allee effect and antipredator feedback. Each panel shows the stability of the feasible coexistence equilibrium $\mathcal{E}^*(\mathcal{X}^*, \mathcal{Y}^*)$ as two parameters vary, with all others fixed at their baseline values $r = 1.2$, $K = 8$, $A = 1.2$, $m = 0.2$, $k = 0.6$, $d = 0.4$, $b = 0.3$, $c = 0.1$, $\varepsilon = 0.05$. Green regions denote local asymptotic stability ($\Re(\lambda_{1,2}) < 0$), pink regions indicate instability, and the black curve marks the Hopf-like boundary defined by $\operatorname{trace}(J(\mathcal{E}^*)) = 0$

7.6. Global stability analysis of the coexistence equilibrium

Theorem 2 already proves global existence, so the symbol $T_{\max}$ in Figure 11 must not be interpreted as the maximal solution lifetime. Here it denotes only the trajectory-local contraction horizon $T_{\max} = \left(\Gamma(1+\alpha)/L\right)^{1/\alpha}$ from the contraction estimate above. For each curve, L is estimated as the largest Jacobian infinity norm sampled along a high-accuracy classical reference trajectory on $0 \leq t \leq 10$. The quantity is therefore a

diagnostic of the local fixed-point interval; a rigorous certificate would require taking the supremum over an enclosing state-space box [22,23,32,42]. Unless noted otherwise, parameters are fixed at $r = 1.0$, $K = 10.0$, $A = 2.0$, $m = 0.5$, $k = 0.8$, $d = 0.3$, $b = 0.2$, $c = 0.1$, $\varepsilon = 0.1$. The sensitivity panels show that this local horizon increases monotonically with α for every displayed parameter value. The largest separation occurs in the prey growth-rate sweep: at $\alpha = 1$, increasing r from 0.5 to 1.5 lowers the horizon from approximately 0.535 to 0.285. The ε, d, and b curves nearly coincide on the chosen trajectory, the k dependence is weak and slightly increasing, and the m dependence is non-monotone. These patterns reflect changes in the sampled Jacobian norm only; they do not imply longer ecological persistence, global stability, or a change in the true existence interval.

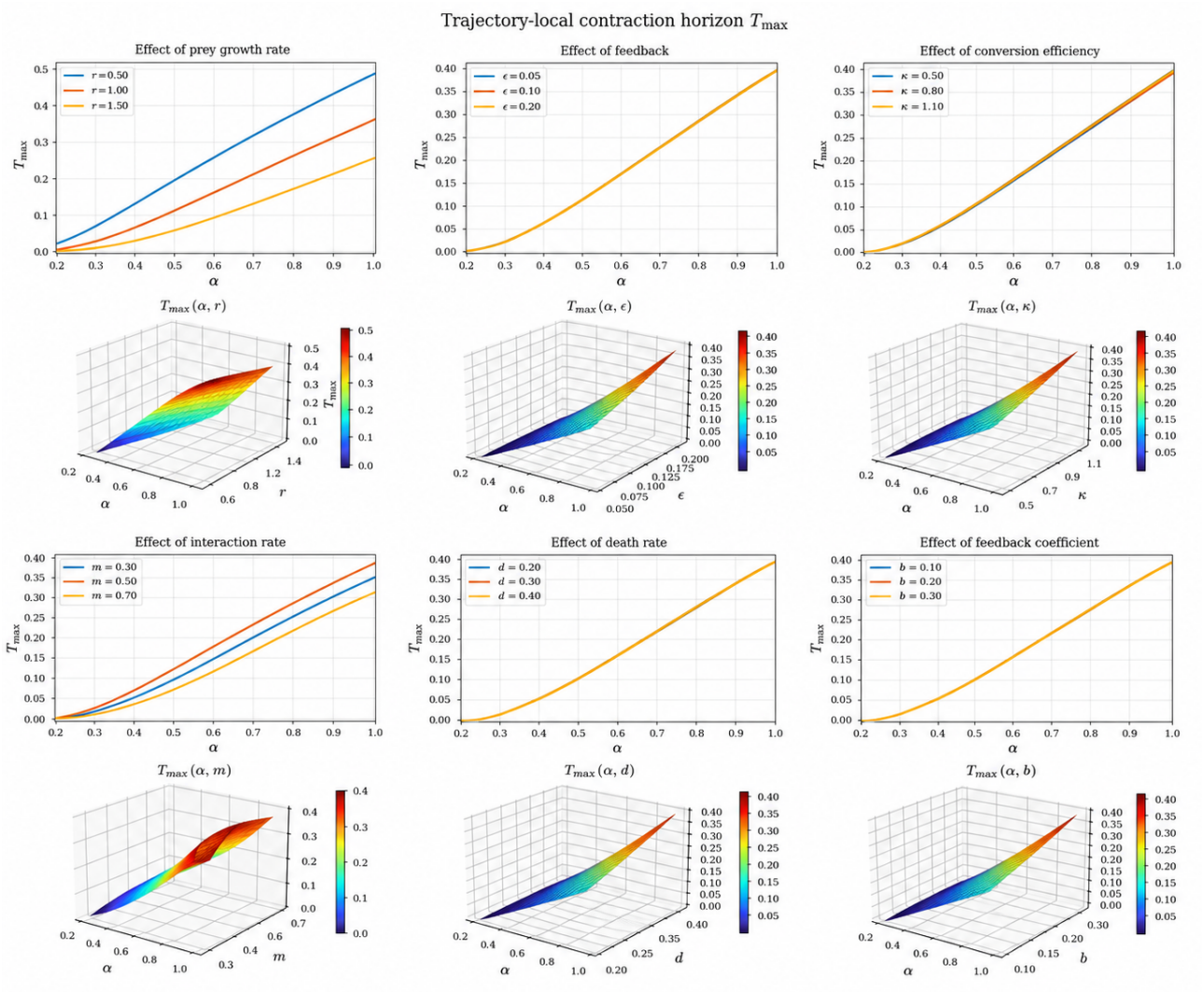

Figure 11. *Sensitivity of maximal existence time $T_{\max}$ with respect to fractional order α and ecological parameters.* The top and middle rows show variation of $T_{\max}$ versus α when each parameter is varied independently, while the 3-D surfaces show combined effects of α with each parameter. Default parameters (unless varied): $K = 10$, $A = 2$, $c = 0.1$, $m = 0.5$, $k = 0.8$, $d = 0.3$, $b = 0.2$, $\varepsilon = 0.1$, $r = 1.0$. Increasing α generally enlarges $T_{\max}$. Higher r or k decreases $T_{\max}$ (destabilizing via faster predation), whereas larger ε or d increases $T_{\max}$. Fractional dynamics ($0 < \alpha < 1$) smooth parameter sensitivity, while $\alpha \to 1$ produces abrupt shifts.

8. Conclusion and future directions

This study develops and analyses a Caputo fractional-order predator–prey (FOPP) model combining a strong prey Allee effect with nonlinear anti-predator feedback. The formulation separates the roles of threshold growth, trophic conversion, feedback saturation, and temporal memory. Quasipositivity establishes

nonnegative solutions, while the weighted quantity $k\mathcal{X} + \mathcal{Y}$ cancels bilinear predation and yields an explicit uniform bound. Local existence therefore extends globally for every nonnegative initial state and $0 < \alpha \leq 1$.

Equilibrium behaviour is determined by a corrected cubic polynomial and explicit filtering by $\mathcal{X}^* \in (A, K)$, $\mathcal{Y}^* > 0$, and $km\mathcal{X}^* - d > 0$. Although the cubic has one or three real algebraic roots, the concave prey nullcline and decreasing convex predator nullcline allow at most two feasible coexistence intersections. The extinction equilibrium E_0 is locally stable for every admissible parameter set, so no coexistence equilibrium can be globally attractive on the entire positive quadrant. The Volterra functional consequently provides a basin-restricted certificate only when its dissipation inequality is verified on a compact positively invariant set. In the fractional setting, the eigenvalue condition

$$|\arg(\lambda_i)| > \tfrac{\alpha\pi}{2}, \qquad 0 < \alpha < 1,$$

is applied to the unchanged Jacobian spectrum: varying α changes the stability-sector threshold and the transient relaxation, not the equilibrium coordinates or eigenvalues.

The ABM–PC implementation is supported by a refinement study with observed orders 1.91, 1.90, and 1.96 for $\alpha = 0.9$, and by an independent $\alpha = 1$ Runge–Kutta comparison with errors below 3.5×10^{-4}. Regenerated simulations show that the first parameter set has no feasible interior equilibrium and approaches extinction, with smaller orders producing a markedly longer finite-time transient. For the second baseline, $E^* = (3.6409, 4.7986)$ is a stable focus at $K = 6$, whereas the carrying-capacity scan becomes unstable from $K = 6.5$ onward. The two-parameter maps also distinguish infeasible, stable, and unstable regions instead of assigning stability to non-biological roots.

For $\alpha = 1$, a trace-zero crossing with positive determinant and transversality is a classical Hopf candidate. For $0 < \alpha < 1$, the analogous Matignon-sector crossing is not a Hopf bifurcation, and exact nonconstant periodic solutions are excluded; oscillations are therefore interpreted as transients. Likewise, the plotted $T_{\max}$ is a trajectory-local contraction horizon, not a maximal existence time, because the solutions are already proved global. These distinctions prevent finite-time persistence and local fixed-point estimates from being overstated as asymptotic stability.

Overall, the corrected model provides a reproducible framework linking memory, Allee thresholds, behavioural regulation, and fractional stability theory. Future work should estimate dimensionally consistent parameters from ecological time series, quantify uncertainty and identifiability, certify basin-restricted Lyapunov inequalities numerically, and extend the model to spatial, delayed, stochastic, or controlled settings only after those empirical checks.

References

[1] Lotka, A. J. (1925). *Elements of Physical Biology*. Williams & Wilkins.

[2] Volterra, V. (1926). Fluctuations in the abundance of a species considered mathematically. *Nature, 118*, 558–560.

[3] Hassell, M. P. (1978). *The Dynamics of Arthropod Predator–Prey Systems* (Monographs in Population Biology, Vol. 13). Princeton University Press.

[4] Maynard Smith, J. (1974). *Models in Ecology*. Cambridge University Press.

[5] Holling, C. S. (1959). Some characteristics of simple types of predation and parasitism. *The Canadian Entomologist, 91*(7), 385–398.

[6] Holling, C. S. (1965). The functional response of predators to prey density and its role in mimicry and population regulation. *Memoirs of the Entomological Society of Canada, 97*(S45), 5–60.

[7] Haque, M. (2009). Ratio-dependent predator–prey models of interacting populations. *Bulletin of Mathematical Biology, 71*(2), 430–452.

[8] Kar, T. K. (2005). Stability analysis of a prey–predator model incorporating a prey refuge. *Communications in Nonlinear Science and Numerical Simulation, 10*(6), 681–691.

[9] Tripathi, J. P., Abbas, S., & Thakur, M. (2015). A density-dependent delayed predator–prey model with Beddington–DeAngelis type function response incorporating a prey refuge. *Communications in Nonlinear Science and Numerical Simulation, 22*(1–3), 427–450.

[10] Wei, F., & Fu, Q. (2016). Hopf bifurcation and stability for predator–prey systems with Beddington–DeAngelis type functional response and stage structure for prey incorporating refuge. *Applied Mathematical Modelling, 40*(1), 126–134.

[11] Huang, Y., Chen, F., & Li, Z. (2006). Stability analysis of a prey–predator model with Holling type III response function incorporating a prey refuge. *Applied Mathematics and Computation, 182*(1), 672–683.

[12] Ma, Z. (2010). *The Research of Predator–Prey Models Incorporating Prey Refuges* [Doctoral dissertation, Lanzhou University].

[13] Ma, Z., Chen, F., Wu, C., & Chen, W. (2013). Dynamic behaviors of a Lotka–Volterra predator–prey model incorporating a prey refuge and predator mutual interference. *Applied Mathematics and Computation, 219*(15), 7945–7953.

[14] Tang, G., Tang, S., & Cheke, R. A. (2014). Global analysis of a Holling type II predator–prey model with a constant prey refuge. *Nonlinear Dynamics, 76*(1), 635–647.

[15] Bianca, C. (2013). Modeling complex systems with particles refuge by thermostatted kinetic theory methods. *Abstract and Applied Analysis, 2013*, Article 152174.

[16] Bianca, C., Dogbe, C., & Guerrini, L. (2014). A thermostatted kinetic framework with particle refuge for the modeling of tumors hiding. *Applied Mathematics & Information Sciences, 8*(2), 469–473.

[17] Allee, W. C. (1931). *Animal Aggregations: A Study in General Sociology*. University of Chicago Press.

[18] Berec, L., Angulo, E., & Courchamp, F. (2007). Multiple Allee effects and population management. *Trends in Ecology & Evolution, 22*(4), 185–191.

[19] Das, S., & Gupta, P. K. (2011). A mathematical model on fractional Lotka–Volterra equations. *Journal of Theoretical Biology, 277*(1), 1–6.

[20] Rivero, M., Trujillo, J. J., Vázquez, L., & Velasco, M. P. (2011). Fractional dynamics of populations. *Applied Mathematics and Computation, 218*(3), 1089–1095.

[21] Elsadany, A. A., & Matouk, A. E. (2015). Dynamical behaviors of fractional-order Lotka–Volterra predator–prey model and its discretization. *Journal of Applied Mathematics and Computing, 49*(1–2), 269–283.

[22] Kilbas, A. A., Srivastava, H. M., & Trujillo, J. J. (2006). *Theory and applications of fractional differential equations* (North-Holland Mathematics Studies, Vol. 204). Elsevier.

[23] Podlubny, I. (1999). *Fractional Differential Equations: An Introduction to Fractional Derivatives, Fractional Differential Equations, to Methods of Their Solution and Some of Their Applications* (Mathematics in Science and Engineering, Vol. 198). Academic Press.

[24] Rayungsari, M., Suryanto, A., Kusumawinahyu, W. M., & Darti, I. (2023). Dynamics analysis of a predator–prey fractional-order model incorporating predator cannibalism and refuge. *Frontiers in Applied Mathematics and Statistics, 9*, Article 1122330.

[25] Zhang, H., & Muhammadhaji, A. (2024). A delayed fractional-order predator–prey model with three-stage structure and cannibalism for prey. *Fractal and Fractional, 8*(8), Article 492.

[26] Gao, W., Tian, X., & Shi, R. (2025). Dynamic analysis and optimal control of a fractional order predator–prey model with economic threshold. *Electronic Research Archive, 33*(8), 4529–4558.

[27] Liu, J., Li, R., & Huang, D. (2025). Stability, bifurcation and characteristics of chaos in a new commensurate and incommensurate fractional-order ecological system. *Mathematics and Computers in Simulation, 236*, 248–269.

[28] Wang, Y., & Meng, X.-Y. (2025). Bifurcation and control of a delayed Leslie–Gower fractional order predator–prey model with fear effect and prey refuge. *Advances in Continuous and Discrete Models, 2025*, Article 103.

[29] Zakirullah, Lu, C., Li, L., Shah, K., Abdalla, B., & Abdeljawad, T. (2025). Mathematical insights into chaos in fractional-order fishery model. *Modeling Earth Systems and Environment, 11*, Article 201.

[30] Sun, X., Li, Y., & Xiao, Y. (2017). A predator–prey model with prey population guided anti-predator behavior. *International Journal of Bifurcation and Chaos, 27*(7), Article 1750099.

[31] Li, Y., Chen, Y. Q., & Podlubny, I. (2010). Stability of fractional-order nonlinear dynamic systems: Lyapunov direct method and generalized Mittag–Leffler stability. *Computers & Mathematics with Applications, 59*(5), 1810–1821.

[32] Rihan, F. A., Lakshmanan, S., Hashish, A. H., Rakkiyappan, R., & Ahmed, E. (2015). Fractional-order delayed predator–prey systems with Holling type-II functional response. *Nonlinear Dynamics, 80*(1–2), 777–789.

[33] Courchamp, F., Clutton-Brock, T., & Grenfell, B. (1999). Inverse density dependence and the Allee effect. *Trends in Ecology & Evolution, 14*(10), 405–410.

[34] Brown, J. S., Laundré, J. W., & Gurung, M. (1999). The ecology of fear: Optimal foraging, game theory, and trophic interactions. *Journal of Mammalogy, 80*(2), 385–399.

[35] Suraci, J. P., Clinchy, M., Dill, L. M., Roberts, D., & Zanette, L. Y. (2016). Fear of large carnivores causes a trophic cascade. *Nature Communications, 7*, Article 10698.

[36] Freedman, H. I. (1980). *Deterministic Mathematical Models in Population Ecology* (Pure and Applied Mathematics, Vol. 57). Marcel Dekker.

[37] May, R. M. (1974). *Stability and Complexity in Model Ecosystems* (2nd ed., Monographs in Population Biology, Vol. 6). Princeton University Press.

[38] Wang, W., Zhu, Y.-N., Cai, Y., & Wang, W. (2014). Dynamical complexity induced by Allee effect in a predator–prey model. *Nonlinear Analysis: Real World Applications, 16*, 103–119.

[39] Tavazoei, M. S., & Haeri, M. (2009). A proof for non-existence of periodic solutions in time-invariant fractional-order systems. *Automatica, 45*(8), 1886–1890.

[40] Ghanbari, B., Günerhan, H., & Srivastava, H. M. (2020). An application of the Atangana–Baleanu fractional derivative in mathematical biology: A three-species predator–prey model. *Chaos, Solitons & Fractals, 138*, Article 109910.

[41] Birkhoff, G., & Rota, G.-C. (1989). *Ordinary Differential Equations* (4th ed.). Wiley.

[42] Diethelm, K. (2010). *The Analysis of Fractional Differential Equations: An Application-Oriented Exposition Using Differential Operators of Caputo Type* (Lecture Notes in Mathematics, Vol. 2004). Springer.

[43] Chattopadhyay, J., & Pal, S. (2002). Viral infection on phytoplankton–zooplankton system—A mathematical model. *Ecological Modelling, 151*(1), 15–28.

[44] Murdoch, W. W., Briggs, C. J., & Nisbet, R. M. (2003). *Consumer–resource dynamics* (Monographs in Population Biology, Vol. 36). Princeton University Press.

[45] Rosenzweig, M. L., & MacArthur, R. H. (1963). Graphical representation and stability conditions of predator–prey interactions. *The American Naturalist, 97*(895), 209–223.

[46] Diethelm, K., Ford, N. J., & Freed, A. D. (2002). A predictor–corrector approach for the numerical solution of fractional differential equations. *Nonlinear Dynamics, 29*(1–4), 3–22.